THESIS/
REPORTS
LOPES, V.L.

EVALUATION OF INTERRILL ERODIBILITY FOR IMPROVED EROSION PREDICTION MODELS

Technical Report to U.S. Forest Service
Intermountain Research Station
Moscow, Idaho

Vicente L. Lopes
and
Peggy Ulman

School of Renewable Natural Resources
310 Bio Sciences East
University of Arizona
Tucson, AZ 85721

Charles H. Luce

U.S. Forest Service
Intermountain Research Station
1221 S. Main
Moscow, ID 83843

Research Joint Venture Agreement No. INT-92716-RJVA
between the U.S. Forest Service Intermountain Research
Service and the University of Arizona

December 1994

FINAL REPORT FOR RESEARCH AGREEMENT
#INT-92716-RJVA
"Evaluation of Interill Erodibility for
Improved Erosion Prediction Models"
UNIVERSITY OF ARIZONA
FS Contact: Charles H. Luce
CoOp Contact: Vicente L. Lopes & Peggy Ulman

EVALUATION OF INTERRILL ERODIBILITY FOR IMPROVED EROSION PREDICTION MODELS

Technical Report to U.S. Forest Service
Intermountain Research Station
Moscow, Idaho

Vicente L. Lopes
and
Peggy Ulman

School of Renewable Natural Resources
310 Bio Sciences East
University of Arizona
Tucson, AZ 85721

Charles H. Luce

U.S. Forest Service
Intermountain Research Station
1221 S. Main
Moscow, ID 83843

Research Joint Venture Agreement No. INT-92716-RJVA
between the U.S. Forest Service Intermountain Research
Service and the University of Arizona

December 1994

EVALUATION OF INTERRILL ERODIBILITY FOR IMPROVED EROSION PREDICTION MODELS

Technical Report to U.S. Forest Service
Intermountain Research Station
Moscow, Idaho

Vicente L. Lopes
and
Peggy Ulman

School of Renewable Natural Resources
310 Bio Sciences East
University of Arizona
Tucson, AZ 85721

Charles H. Luce

U.S. Forest Service
Intermountain Research Station
1221 S. Main
Moscow, ID 83843

Research Joint Venture Agreement No. INT-92716-RJVA
between the U.S. Forest Service Intermountain Research
Service and the University of Arizona

December 1994

ABSTRACT

Soil loss was measured on selected unsurfaced forest roads in Idaho and Colorado, using a Purdue-type rainfall simulator. From the data collected, both flow-induced and raindrop-induced interrill erodiblity parameters were determined. Each forest road site consisted of one $5m^2$ plot and two $1m^2$ plots which simultaneously received artificial rainfall. Soil loss from the small plots was due solely to detachment by raindrops. The larger $5m^2$ plots may include some flow-induced soil loss. A method was developed to apportion the erosion from the $5m^2$ plots between flow-induced and raindrop-induced soil loss. Four different models of raindrop-induced erodibility and three different models of flow-induced erodibility were compared. Those considered most applicable to forest road conditions were suggested for further use in an erosion model for disturbed forestlands. This study serves as an important contribution in developing such a model by providing initial estimates of interrill erodibility parameters for forest road conditions.

Keywords: soil erodibility, forest roads, erosion models

TABLE OF CONTENTS

Page

LIST OF ILLUSTRATIONS....v

LIST OF TABLES....vi

ACKNOWLEDGEMENTS....vii

INTRODUCTION....1

Objectives....3

Scope of Report....5

LITERATURE REVIEW....6

Hillslope Erosion Processes....6

Estimation of Erodibility Parameters....7

METHODOLOGY....10

Data Collection....10

Field Data Collection....10

Laboratory Soil Analyses....14

Determination of Parameters....16

Rain-induced Erodibility Parameter....17

Predicting Interrill Erodibility....21

Estimation of Flow-induced Erodibility Parameter....24

Theory....24

Models of Flow-induced Erodibility....25

Fundamental Equations....26

TABLE OF CONTENTS -- Continued

RESULTS AND DISCUSSION....30

Soil Characteristics....30

Soil Gradation Comparisons - Dispersed vs. aggregated particle size analysis....30

Organic Matter....31

Volumetric Water Content....31

Clay Mineralogy....32

Rain-induced Erodibility....34

Comparisons of Equations....34

Predicting Interrill Erodibility....41

Flow-induced Erodibility....48

Determination of Flow-induced Sediment Discharge....48

Flow Characteristics....51

Evaluation of Models....56

Summary....59

CONCLUSIONS AND RECOMMENDATIONS....60

REFERENCES....62

APPENDICES....66

A. Dispersed Versus Aggregated Particle Size Analysis....67

B. Fitted Sediment Transport Models....73

TABLE OF CONTENTS -- Continued

C. Governing Equations for Sediment Transport Using a Coupled Flow and Raindrop Impact Detachment Model.....78

LIST OF ILLUSTRATIONS

Figure		Pages
1	Example of plot layout on the road surface	12
2	Comparison of interill erodibility equations	39
3	Rainfall intensity versus rainfall excess rate	40
4	Estimated versus predicted interill erodibility, K_i, for the $1m^2$ plots at all study areas	46
5	Graphical determination of critical shear velocity	55

LIST OF TABLES

Table		Pages
1	Location of rainfall simulation sites and summary soil information	10
2	Nominal rainfall intensity, mean particle size and plot slope	11
3	Results of soil analyses	33
4	Empirical interill erosion equations	34
5	Computations for $1m^2$ plot interrill erodibility parameter	38
6	Regression equation variables and resulting predicted interrill erodibility parameter, K_{io}, from equations (12) and (13)	45
7	Regression equation variables and resulting predicted interrill erodibility parameter, K_{io}, from equations (14a) and (14b) using both dispersed and undispersed silt+clay	45
8	Estimated and predicted interrill erodibility values	47
9	Sediment discharge for $5m^2$ plots	50
10	Flow parameters for $5m^2$ forest road plots	53
11	Shear stress and stream power estimates	54
12	Flow-induced erodibility equations	56
13	Flow-induced erodibility parameters for wet and very wet runs	58

ACKNOWLEDGEMENTS

The authors wish to express their gratitude to the personnel of the USDA Forest Service Intermountain Research Station, Moscow, Idaho who made this study possible. Charles Luce provided technical support for the project. His assistance and guidance in completing the report are greatly appreciated.

The USDA Agricultural Research Service, Tucson, Arizona, provided laboratory facilities for the completion of soil analyses.

Dr. Edward R. Burroughs recognized the need for versatile erosion prediction tools in forest environments. This project arose from his study of forest road erodibility which was his personal research topic at the time of his death.

INTRODUCTION

Soil erosion involves the detachment and transport of individual soil particles due to the forces of raindrop impact and flowing water. Under undisturbed conditions this process occurs at a natural rate; however, when severe soil disturbance occurs, erosion rates accelerate. Undisturbed forestlands are generally considered to be areas of low erosion potential due to the high rates of interception, infiltration and evapotranspiration associated with dense forest cover. Any disturbance or management activity that removes vegetative cover and exposes mineral soil foreshadows a potentially high rate of surface erosion. Examples of such disturbances in forestlands include timber harvesting, fire, and road construction. Timber harvesting usually results in minor erosion since a relatively small portion of the land surface is disturbed in a logging operation, and fire-induced soil erosion is variable depending on the intensity of the burn and the amount of ground litter removed (Rice et al, 1972). However, the construction, use, and maintenance of dirt roads in forests creates substantial increases in soil loss (Hoover, 1945; Trimble and Weitzman, 1953; Bilby, 1985; Megahan et al., 1991). Road construction disturbs soil, vegetation, slope gradient and drainage patterns, and creates the potential for accelerated erosion and increased sediment yield.

One of the primary concerns related to increased soil loss from forest roads is the delivery of sediment to nearby streams. The headwaters of most rivers in the western United States are located in national forests, and these rivers carry more than half of the

annual runoff for the western states (Wilkinson and Anderson, 1987). The physical quality of streamflow is largely determined by the amount of sediment that it carries. Downstream users, including western municipalities, rely on the national forest watersheds for a dependable flow of clean water.

Aquatic ecosystems can be adversely impacted when sediment enters a stream. Suspended sediment restricts sunlight from reaching photosynthetic aquatic plants. Deposited sediment in streambeds smothers benthic communities and covers gravel which serves as important spawning habitat, especially for salmonid fishes (Bilby, 1985). As well as serving as vital aquatic habitat, rivers, streams and lakes serve are also important recreational and aesthetic resources whose value is diminished when sediment concentrations are high.

Land managers require erosion prediction tools to assist in the selection of low impact management alternatives that reduce soil erosion and minimize damage to mountain streams. The most recent trend in erosion prediction research explores the use of versatile erosion models that provide insight into the physical processes involved. Water runoff, erosion and sediment yield are hydraulic and hydrologic phenomena governed by complex physical processes. Mathematical models can be constructed to simulate these complex processes and predict the amount of soil loss from a land surface.

Objectives

The primary goal of this study is to contribute to the development of a process-based erosion model applicable to forest road conditions. The U.S. Department of Agriculture Water Erosion Prediction Project (WEPP) was initiated "to develop new generation water erosion prediction technology for use... in soil and water conservation and environmental planning and assessment" (Lane and Nearing, 1989). The computer model for WEPP is intended to apply to all situations where water erosion occurs, including that resulting from rainfall, snowmelt and irrigation on croplands, rangelands, forestlands and land disturbed by construction and mining. The model was originally developed using data collected from agricultural lands. Modifications gave rise to a model suitable to rangelands; additional modifications are necessary to make the model applicable to forest conditions. The U.S. Forest Service is involved in developing a "forest component" for WEPP which will account for many of the hydrologic and erosion conditions unique to forestlands (Burroughs et al., 1991). Since roads are a significant source of sediment in forest environments, they receive priority attention in developing the forest model.

In order to apply existing process-based erosion prediction models to forest roads, the model parameters must first be estimated. One of the parameters must reflect the inherent susceptibility of the soil to erode under rainfall conditions. The soil erodibility parameter indicates the ease with which soil is detached by splash during rainfall or by the shear of surface flow. This study will identify the soil erodibility parameters for a steady

state process-based model using experimental soil loss data collected from forest road plots.

Soil erodibility parameters are not fundamental properties (Nearing et al., 1990); they cannot be measured directly. These parameters depend on the formulation of the detachment equations in the erosion model. This study proposes several alternative detachment equations for forest road conditions and tests them to verify which are most applicable. The erodibility parameter values determined through the use of these equations will be referred to as 'estimated' or 'computed'.

After the appropriate term for erodibility has been fitted using an experimental data set, the next logical step in analyzing erodibility is to regress the fitted parameter against measurable soil properties. This allows the erodibility parameter to be predicted for sites where rainfall simulation experiments have not been conducted. Regression equations relating erodibility to soil properties have previously been developed for other land types, and three of those equations which predict interrill erodibility will be examined using forest road data.

The specific objectives related to the overall goal of this study were to:

1. Compute the soil erodibility parameters using an experimental data set collected on forest roads.
2. Compare the computed parameter values to the values predicted by existing regression-type soil erodibility equations.
3. Compare sediment transport equations for flow-induced erosion on interrill areas.

Scope of Report

Forest land managers must be able to accurately predict the amount of soil loss resulting from alternative road construction and maintenance designs and anticipate the corresponding effect on nearby streams in order to develop and evaluate management plans. This study serves as an important contribution in developing a process-based erosion model for forest roads by providing initial estimates of the erodiblity parameters for forest road conditions.

This report is an analysis of the rainfall-runoff and erosion data collected from four study areas on forest roads using a small area simulator. Primary data collection methods are presented. Results of data analyses related to the study's goals and objectives are given.

LITERATURE REVIEW

Hillslope Erosion Processes

Process-based models assume that the erosion processes are understood and can be represented mathematically to simulate the actual processes. Due to the complexity of the erosion process, some simplifying assumptions are made in describing sediment detachment, transport, and deposition. Usually the erosion process is divided into two phases based on the characteristics of overland flow (Meyer et al., 1975). These phases are termed interrill and rill erosion. After the rainfall rate exceeds the soil's infiltration capacity and surface storage has been satisfied, overland flow begins. Initially overland flow is very shallow and erosion related to this type of flow is termed interrill erosion. As overland flow moves downslope and increases in depth, it tends to concentrate in small channels called rills. Natural variations in soil erodibility and changes in microtopography trigger rill formation. Soil loss resulting from the flow in these small channels is called rill erosion. All soil loss from the forest road plots discussed in this report are assumed to be part of the interrill phase of erosion.

Rainfall and runoff play roles in both detaching and transporting soil particles. Attempts have been made to clearly define those roles in both the interrill and rill phases of erosion in order to provide a conceptual framework for models of sediment removal. In some models of interrill erosion, raindrop impact is responsible for all detachment and surface flow alone is responsible for sediment transport (Foster and Meyer, 1972);

however, this may be an over-simplification of the mechanics of sediment removal in interrill overland flow. For example, the momentum imparted by a raindrop striking the soil surface in an interrill area at terminal velocity not only detaches soil particles from the soil mass, but also transports them relatively short distances in splash water. Broad shallow overland flow is more efficient at transporting sediment as compared to raindrop impact, but its hydraulic characteristics in interrill areas prove its capability for detachment (Parsons and Abrahams, 1992; Govers, 1987). The depth of the surface water layer also influences the detachment ability of rainfall. Kinnell and Wood (1992) showed that the raindrop detachment rate became minimal when the depth of ponded water was greater than 4 mm.

In combination, rainfall and runoff provide the kinetic energy to erode soil materials. Because these energy inputs exist on a continuum, it is difficult to precisely separate detachment and transport processes when analyzing soil erosion data. Instead, a balance between the two is found by analyzing data from different rainfall intensity and overland flow rate experiments.

Estimation of Erodibility Parameters

An important step in the development of an erosion model is the estimation of parameter values. A parameter is a numerical measure of a property or characteristic that is constant for a system or process under specified conditions. The parameter values of

concern in this study reflect the soil erodibility, the inherent susceptibility of the soil to erode. Parameter estimation is a two-stage process. First, the parameter values must be identified using the computer model and field data. Then the identified model parameter is related to measurable variables such as soil texture, organic matter content, etc. This second step is necessary to make the model useable for applications under situations different from those for which the model was developed.

In many studies, erosion model parameters are identified by physical reasoning, or are found by fitting observed data using optimization techniques. Because of the difficulty of obtaining detailed field measurements of flow depths, velocities and other variables necessary to estimate individual parameters by physical reasoning, optimization procedures are considered advantageous (Blau et al., 1988). For this procedure, a least squares objective function is used to describe the difference between predicted and measured field values of sediment load. Optimizing involves minimizing this objective function for a set of field data.

Due to the impracticality of identifying actual erodibility parameter values for all soil types, the determination of soil properties related to erodibility has been the topic of many studies. Early work concentrated on the ability to qualitatively define the degree of potential soil erodibility. For example, Middleton (1930) categorized soils as erodible or non-erodible based on a "dispersion ratio" comparing the amount of silt + clay in an undispersed sample to that in a dispersed sample. Soils with a dispersion ratio greater than 15% were considered to be erodible.

Process-based erosion prediction technology requires a quantitative estimate of soil erodibility which is relevant to the prediction model. Researchers have attempted to develop regression equations to predict erodibility that are relevant to a particular model. Elliot et al. (1989) correlated the erodibility parameters used in the WEPP model to a variety of physical and chemical properties, and complex regression equations were developed to predict the erodibility of croplands using these properties. Of the nineteen soil properties included in that study, no single property correlated strongly to the observed variations in soil erodibility.

Data about certain soil variables such as specific surface area and cation exchange capacity are not readily available for rangelands and forestlands due to the relatively small amount of study wildland soils have received in the past in comparison with agricultural lands. Simpler regression equations based on easily measured soil variables have been developed to predict the interrill erodibility of rangelands for the WEPP model (Alberts et al., 1989; Flanagan, 1991). Texture, organic matter and volumetric water content are the factors included in those equations.

METHODOLOGY

Data Collection

Field Data Collection

This study uses data collected by the U.S.D.A. Forest Service Intermountain Research Station during soil erosion experiments conducted on forest roads. The roads were unsurfaced; no gravel or asphalt had been applied to the traveled surface. Since the condition of each road varied slightly due to the amount of traffic using the road, the time elapsed since construction and level of maintenance, the road surfaces were graded to create a standard initial condition prior to the experiments. Four different study areas are examined in this study, three in Idaho and one in Colorado. Each study area represents a different type of soil. More specific information concerning the location of each study area and a general characterization of the soil is given in Table 1. For each study area, two or more sites were selected for investigation. At the selected sites, bordered plots were installed on the road surface, and a Purdue-type simulator was used to apply artificial rainfall to the plots. The Purdue simulator is based on an oscillating nozzle concept; the

Table 1. Location of rainfall simulation sites and summary soil information.

Study Area	Location	Year	Parent Material	Surface Soil Texture
Deep Creek	Lemhi County,ID	1989	Metamorphic -Gneiss	sandy loam
Hahn's Peak	Routt County, CO	1989	Eolian Sandstone	coarse sandy loam
Tin Cup Creek	Caribou County, ID	1989	Metamorphic - Shale	loam
Potlatch River - Tee Meadow	Latah County, ID	1990	Loess	silt loam

simulator's design is described by Foster et al. (1979).

Each site consisted of three plots: one large 1m x 5m plot and two smaller 1m x 1m plots. Figure 1 presents an example of a hypothetical plot layout. In some experiments one of the 1 m^2 plots was covered with window screen to dissipate the energy of raindrop impact; data from those plots were not employed for this study. All plots were installed on a freshly graded road surface. Sidewalls made of sheet metal provided the borders of the plots and were oriented parallel to the direction of flow across the road surface. The rainfall simulator was positioned above the plots, and rainfall was applied at a given intensity. Runoff and sediment were collected at a headwall at the lower end of the plot. The sidewalls and headwalls were sealed to the surface of the road with bentonite. Table 2 provides more specific information on the topography of the plots, the nominal rainfall intensity applied and the mean particle size (D_{50}) of the < 2-mm fraction of the surface soil horizon.

Table 2. Nominal rainfall intensity, mean particle size and plot slope.

Site	Nominal Rainfall Intensity (mm hr^{-1})	Surface Soil D_{50} (mm)	Slope (%)		
			Plot 1 1m x 5m	Plot 2 1m x 1m	Plot 3 1m x 1m
Deep Creek 1	30	0.201	5.68	6.50	6.62
Deep Creek 2	50	0.201	5.92	6.89	6.23
Deep Creek 3	30	0.156	1.80	3.63	4.16
Hahn's Peak 1	30	0.215	8.77	---	8.73
Hahn's Peak 2	50	0.215	4.70	---	4.35
Tin Cup Creek 1	30	0.053	8.49	---	7.70
Tin Cup Creek 2	50	0.053	13.45	---	11.82
Potlatch River 3	50	0.018	5.12	---	4.92
Tee Meadow 5	50	0.018	6.53	---	7.28

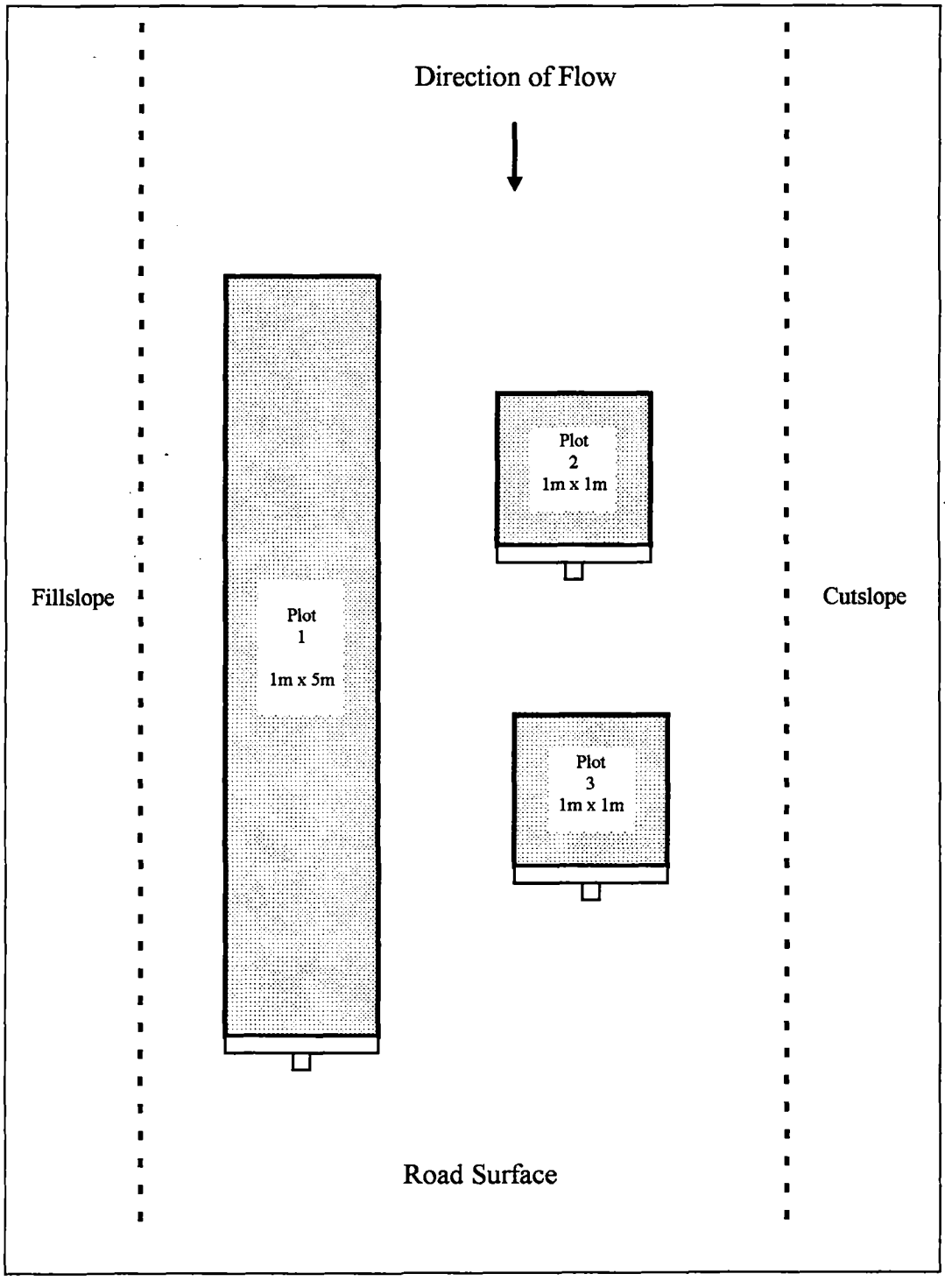

Figure 1. Example of plot layout on the road surface.

Each experiment consisted of three separate 30-minute simulated rainfall events. The events were designated as dry, wet and very wet. Following the dry run at existing soil moisture conditions, the plots were covered for 24-hours to reduce evaporation, then the wet run was simulated. The very wet run occurred approximately 1 hour following the wet run. Because this study uses erosion equations based on the assumption of steady state flow, only data from the wet and very wet were considered. The wet and very wet runs reach conditions close to equilibrium (steady state); the initial dry runs do not always meet this criterion. The rainfall intensity was measured before and after each run by covering the plots with sheet metal covers and measuring the runoff from the impermeable surface. Rainfall was set at a nominal intensity of either 30 mm hr^{-1} or 50 mm hr^{-1}. The uniformity of application during each event was evaluated with rain gauges located regularly around the plots.

Data collected from each plot include flow rate, sediment concentration, soil moisture and bulk density. Sediment-laden runoff samples were collected at 45-second intervals from the headwall of each plot. The flow rate was calculated by dividing the volume of each sample by the time required to collect the sample. One-half of the samples were designated as "sediment" samples. Each sediment sample was evaporated in a large oven. The volume of the sample and the weight of sediment measured after drying was used to calculate sediment concentration. The other half of the samples were designated as "rate" samples. The volume of these samples was measured in the field. In 1989, these volumes were measured with a graduated cylinder; in 1990, a scale was used to indirectly

measure volume. Gravimetric soil moisture samples were collected at established markers outside the plots at the following four times: prior to and immediately following the dry run, before the wet run and immediately after the very wet run. The compliant cavity method (Grossman and Pringle, 1987) was used to measure bulk density of soil inside each plot following the very wet event.

Laboratory Soil Analyses

Surface composite soil samples were collected at the time of fieldwork from each rainfall simulation site by removing the upper 2.5 cm of soil and rocks from a designated area of the road. A separate sample was collected to represent each site except when two sites were immediately adjacent and could be adequately represented with one sample. Each surface composite was air-dried and stored in plastic-lined canvas bags until the time of analysis.

The analyses of clay mineralogy, volumetric water-holding capacity, organic matter content, dispersed particle size and water stable aggregates described below were conducted using representative samples taken from each surface composite and screened through a 2-mm mesh. Soil was not forcibly pushed through the sieve and aggregates were not broken up. X-ray diffraction of the clay portion of each of the soils used in this study was conducted at the Soil Conservation Service (SCS) National Soil Survey Laboratory in Lincoln, Nebraska, and provided estimates of the relative amounts of clay

minerals. Percentages of slected clay minerals were interpreted from relative peak size patterns. These were then expressed as percentages of the total clay fraction. The clay mineral percentages were calculated for use in existing erodibility prediction equations.

The volumetric water content was determined using standard laboratory procedures for disturbed soil samples (Richards, 1965). Three replications of the < 2 mm fraction of each soil sample were placed on a porous ceramic plate in a pressure chamber, 0.033 MPa of pressure were applied, and measurements of saturated volumetric water content were taken after a two-week equilibration period.

The Walkley-Black (1934) rapid titration method was employed to determine the organic matter content of three replications of each sample. This method involves the oxidation of organics by chromic acid with subsequent titration.

The particle size analysis was conducted using both dispersed and aggregated techniques. Results of the dispersed textural analysis were provided by the SCS National Soil Survey Laboratory in Lincoln, Nebraska, using standard methods (USDA-SCS, 1992). Yoder (1936) originally suggested a wet-sieving technique for determining aggregate stability which was later modified (Kemper and Koch, 1966; Kemper and Rosenau, 1986). The methods employed for measuring aggregated particle size fractions in this study are described by Burroughs et al. (1992). The aggregate sieving apparatus used in this analysis is described by Kemper and Rosenau (1986). The apparatus is designed to agitate eight small sieves in individual water baths. Six different sieve sizes were used to analyze each soil: #6 (1.18 mm openings), #30 (0.6 mm), #50 (0.3 mm),

#100 (0.15 mm), #200 (0.075 mm) and #270 (0.05 mm). A measured amount of soil which differed according to sieve size was added to each sieve. For the #16 and #30 sieves, 4.2 to 4.6 g was used; 2.0 to 2.5 g were used for the #30 and #50 sieves, and 1.0 to 1.5 g were used in the #200 and #270 sieves. The results of all sieve sizes are shown in Appendix A; however, only the results from the #270 sieve size are further used in this study as the division between sand versus silt and clay.

Burroughs et al. (1992) point out that hydrophobic soils influence the measurement of aggregation as determined by this method due to their tendency to repel water penetration. Therefore, prior to analyzing water stable aggregation, a preliminary water drop penetration test was conducted on each soil to determine the repellency of the soils. With all of the penetration times lasting 3 seconds or less, none of the soils in this study were determined to be repellent.

Determination of Parameters

The one-dimensional sediment continuity equation governing most transient process-based erosion models on broad shallow flow areas is given as:

$$\frac{\partial(ch)}{\partial t} + \frac{\partial(cq)}{\partial x} = D_f + D_i \qquad (1)$$

where h = local flow depth, m
c = sediment concentration, kg m^{-3}
q = unit flow discharge, m^2 s^{-1}
D_f = detachment (or deposition) rate due to flow, mass per time per unit area, kg s^{-1} m^{-2}
D_i = detachment rate of particles due to raindrop impact, mass per time per unit area, kg s^{-1} m^{-2}
x = distance downslope, m
t = time, s.

The term $\frac{\partial(ch)}{\partial t}$ represents the storage rate of sediment within the flow depth, and $\frac{\partial(cq)}{\partial x}$ denotes the buildup or loss of sediment with distance. The steady-state approximation to equation (1) is (Foster and Meyer, 1972):

$$\frac{dG}{dx} = D_i + D_f \tag{2}$$

where G = cq = sediment load, mass per time per unit width, kg s^{-1} m^{-1}.

Rain-induced Erodibility Parameter

Soil loss in the 1 m^2 plots is assumed to be due solely to raindrop impact. Data collected from that plot size will be used to determine the rain-induced erodibility parameter. Four different empirical interrill equations were used for estimating rain-induced erodibility. The first two equations relate interrill detachment to rainfall intensity. The second two equations relate interrill detachment to both rainfall intensity and rainfall excess rate. For both cases, one equation is tested which also includes a term accounting for the effect of slope on interrill detachment. The interrill erodibility parameter is

identified with the symbol, Ki. Because the value of this parameter depends in part on the form of the erosion equation used, the interrill erodibility parameter is identified with a unique symbol for each equation. For each equation, the rate of soil material discharged across a unit width of the downslope boundary of an interrill area is given by :

$$q_{sr} = D_i \; L \tag{3}$$

where q_{sr} = rain-induced sediment discharge (mass of soil material per unit width per unit time), kg m^{-1} s^{-1}
D_i = interrill detachment rate, kg m^{-2} s^{-1}
L = slope length, m.

The first interrill erosion equation used in this study was originally presented by Meyer and Wischmeier (1969). They proposed that soil detachment by rainfall is proportional to the square of rainfall intensity, or:

$$D_i = Ki_1 \; i^2 \tag{4}$$

where Ki_1 = rain-induced interrill erodibility factor, kg s m^{-4}
i = rainfall intensity, m s^{-1}.

Combining equations (3) and (4) yields

$$Ki_1 = \frac{q_{sr}}{i^2 L} \tag{5}$$

Elliot et al. (1989) analyzed a series of interrill erosion experiments to determine the interrill erodibility (K_i) of a number of cropland soils within the Water Erosion Prediction Project (WEPP). This analysis was based on the equation

$$D_i = Ki_2 \; i^2 \; S_f \tag{6}$$

where S_f = slope factor, dimensionless.

Equation (6) represents the second equation to be tested for its applicability to forest road erosion conditions. From an analysis of previous studies, Liebenow et al. (1990) concluded that

$$S_f = 1.05 - 0.85 \exp(-4 \sin\theta) \tag{7}$$

where θ = slope angle, degrees.

This equation resulted in a coefficient of determnation of 0.96 for cropland data. In this relationship, S_f decreases as slope gradient increases. This decreasing response to slope gradient can be attributed to a change from transport-limited to detachment-limited conditions as slope gradient increases (Foster, 1982). Combining equations (3) and (6) yields

$$Ki_2 = \frac{q_{sr}}{i^2 S_f L} \tag{8}$$

The inclusion of the slope factor recognizes the significant effect that slope plays on erosion in steep hillslopes.

Equation (4) is a simple functional form of detachment by raindrop impact which incorporates rainfall intensity, i, as a measure of the erosivity of raindrop impact. If the rate of detachment is related to rainfall intensity squared, and the flow transport capacity is related to the ratio of rainfall excess to rainfall intensity (Lane and Shirley, 1985), then a simple form of the interrill equation is

$$D_i = Ki_3 i^2 \left(\frac{r}{i}\right) = Ki_3 ir \tag{9}$$

where r = rainfall excess, m s^{-1}.

Equation (9) is the current formulation for interrill detachment used in the rangeland option of the WEPP model (Flanagan, 1994). From equations (3) and (9),

$$Ki_3 = \frac{q_{sr}}{irL} \tag{10}$$

Including the slope factor given by equation (7) with the interrill detachment equation reflected in equation (9) results in

$$Ki_4 = \frac{q_{sr}}{irS_fL} \tag{11}$$

Predicting Interrill Erodibility

Due to the expense and time involved in determining model parameters using rainfall simulation experiments, it is a common practice to develop regression equations that relate model parameters to measurable site soil properties. These regression equations can then be used to predict parameter values without experimental erosion data. Several regression equations have been developed to estimate interrill erodibility based on soil properties. The estimated parameter values identified using equation (9) will be compared to the predicted parameter values using three previously developed regression equations.

The first two equations are similar and were developed for rangelands in conjunction with the WEPP program. The first equation (Alberts et al., 1989) is given as:

$$Ki_{p1} = 1000\,(1709 - 1765\,S_a - 645\,S_i - 4457\,O_m - 902\,\theta_{fc}) \tag{12}$$

$$r^2 = 0.91$$

The second equation (Flanagan, 1991) is a revised version of the first:

$$Ki_{p2} = 1000\ (3042 - 3166\ S_a - 8816\ O_m - 2477\ \theta_{fc}) \qquad (13)$$

$$r^2 = 0.94$$

where S_a = fraction of sand (0 to 1),
S_i = fraction of silt (0 to 1),
O_m = fraction of organic matter (0 to 1),
θ_{fc} = volumetric water content at 0.033 MPa, ($m^3\ m^{-3}$).

Another equation for comparison was derived by Burroughs et al. (1992). This equation estimates interrill erodibility as:

$$Ki_{p3} = 1000\ (-25.7 + 69.2\ (Si + Cl) - 0.6\ (Si + Cl)^2 - 34.3\ (Ka) + 86.0\ (Sm) \qquad (14a)$$

$$r^2 = 0.91$$

where Si + Cl = dispersed percent silt plus percent clay,
Ka = percent kaolin clay present in the soil,
Sm = percent smectite clay present in soil.

This equation will be applied in two different forms. The first is identified as equation (14a) and uses a dispersed measure of silt plus clay (Si + Cl). The second, equation (14b), uses an undispersed or aggregated measure of silt + clay (si + cl).

$$Ki_{p4} = 1000\,(-25.7 + 69.2\,(si + cl) - 0.6\,(si + cl)^2 - 34.3\,(Ka) + 86.0\,(Sm) \qquad (14b)$$

The erodibility parameters used in process-based models are not solely a function of soil properties, but are dependent on the form of the detachment equation used in the model. The interrill detachment equation in the WEPP model was originally given as shown in equation (8) (Lane and Nearing, 1989). Subsequently the form of that equation was modified to equation (10). The erodibility prediction equations given here (equations (12), (13), (14a) and (14b)) were developed in conjunction with the previous formulation of interrill detachment (equation (8)). It is not possible to directly compare the parameter values predicted with these equations to the parameter values determined using the new interrill erosion equation (equation (10)). However, it is possible to convert Ki values given by equations (12), (13), (14a) and (14b) to values consistent with the new interrill erodibility parameters as shown here:

$$ki_{pn} = Ki_{pn}\left(\frac{i}{r}\right)S_f \qquad \text{for } r > 0 \qquad (15)$$

where ki_{pn} = predicted parameter values based on equation (10), n = 1, 2, 3, 4.
Ki_{pn} = K_i values predicted by equations (12), (13) and (14a) and (14b) based on equation (8).

Estimation of Flow-induced Erodibility

Theory. In order to quantify the erodibility associated with flow, the soil loss due to raindrop impact must be theoretically separated from the soil loss caused by flow. Guy et al. (1987) and Guy et al. (1992) described the equilibrium transport capacity of rain-impacted broad shallow flow on a uniform plane as:

$$q_{st} = q_{sf} + q_{sr} \tag{16}$$

where q_{st} = total transport capacity of rainfall-disturbed flow, kg m^{-1} s^{-1}

q_{sf} = runoff contribution to transport capacity, kg m^{-1} s^{-1}

q_{sr} = raindrop impact contribution to transport capacity, kg m^{-1} s^{-1}

Soil loss in the 1 m^2 plots is assumed to be due solely to raindrop impact so that $q_{sf} = 0$. Therefore, the rainfall-induced sediment discharge is equal to the total sediment discharge for the small plots ($q_{sr} = q_{st}$). The previous section described the calculation of the interrill erodibility parameter, K_i, using the measured soil loss, runoff discharge and rainfall intensity in conjunction with equation (10).

The larger 5 m^2 plots may include some flow-induced soil loss as well as interrill erosion. Since neither the flow-induced nor the rainfall-induced soil loss was measured separately on the large plots, some assumptions must be made in apportioning the total soil loss between the two categories. The interrill erodibility parameter associated with the small plots also applies to the corresponding larger plots. Each site in this study consists of one 5 m^2 plot and at least one 1 m^2 plot which simultaneously received artificial

rainfall; in some cases, data from two 1 m^2 plots are available. When there is data from two small plots, the geometric mean of the interrill erodibility parameter calculated for each small plot was taken. Using the interrill erodibility parameter from the small plot and the measured runoff discharge and rainfall intensity from the large plot, q_{sr} can be calculated using equation (10). The runoff contribution to transport capacity, q_{sf}, can be calculated as the difference between the total measured sediment discharge and the rain-induced contribution to transport capacity.

Models of Flow-induced Erodibility. Three models of flow-induced sediment detachment and transport are presented here and tested for their applicability to forest road conditions. The first equation described by Govers (1992), relates flow-induced erosion to excess effective stream power as

$$q_{sf} = Kf_l (\Omega_e)^b \tag{17}$$

where Kf_l = flow-induced erodibility parameter
Ω_e = excess effective stream power
b = exponent.

The concept of excess effective stream power is defined by Bagnold (1980) as

$$\Omega_e = \Omega - \Omega_c \tag{18}$$

where

$$\Omega = \text{effective stream power} = \frac{(\tau\bar{u})^{3/2}}{h^{2/3}} = \frac{(\gamma h S\bar{u})^{3/2}}{h^{2/3}} \tag{19}$$

$$\Omega_c = \text{critical stream power} = \frac{(\tau_c\bar{u})^{3/2}}{h^{2/3}} = \frac{(\rho(\bar{u}_{*_c})^2\bar{u})^{3/2}}{h^{2/3}} \tag{20}$$

ρ = specific density of fluid, kg/m^3
γ = specific weight of fluid, $N\ m^{-3}$
$\bar{u}$ = mean flow velocity, $m\ s^{-1}$

h = flow depth, m
$\bar{u}_{*c}$ = mean critical shear velocity, m s^{-1}
S = ground-surface slope gradient.

Flow-induced erosion can also be related to the shear stress of flow. Using an equation similar in form to equation (17) results in

$$q_{sf} = Kf_2 (\tau_e)^b. \tag{21}$$

Govers (1992) included a particle diameter term with shear stress to reflect the influence of particle size in sediment transport capacity. That equation is

$$q_{sf} = Kf_3\left(\frac{\tau_e}{D^{.33}}\right)^b \tag{22}$$

where D = particle diameter, m.

Equations (21) and (22) are based on the concept of excess effective shear stress defined as

$$\tau_e = \tau - \tau_c \tag{23}$$

where τ_e = excess effective shear, N m^{-2}
τ = shear stress, N m^{-2}
$= \gamma h S$
τ_c = critical shear, N m^{-2}
$= \rho u_{*c}^2$

Fundamental Equations. Presented here is an algorithm to aid in the calculation of the variables used in the stream power and shear stress models. Variables such as depth of flow and shear velocity were not measured directly from the experimental road plots; however, they can be evaluated indirectly from other measured variables.

Since the amount of flow or discharge was measured, it can be used as a starting point. An important characteristic of flow is the Reynolds number, Re, which expresses the ratio of inertial forces to viscous forces. The Reynolds number is given as

$$Re = \frac{\bar{u}h}{\nu} = \frac{q}{\nu} \tag{24}$$

where q = unit discharge, $m^2\ s^{-1}$
ν = kinematic viscosity, $m^2\ s^{-1}$.

Analysis of surface runoff on forest roads requires the identification of hydraulic roughness coefficients. Non-transportable flow obstacles like stones and soil clods increase the hydraulic roughness and simultaneously reduce the erosivity and transporting capacity of flow (Govers, 1992). The Darcy-Weisbach friction factor, f, is often used for broad shallow flow and is defined as

$$f = \frac{8ghS}{\bar{u}^2} \tag{25}$$

where g = gravitational acceleration, $m\ s^{-2}$

It can also be estimated using the association of f and Re according to the following relationship:

$$f = \frac{K}{Re} \tag{26}$$

By combining equations (24) and (26), the following results:

$$f = \frac{K\nu}{q} \tag{27}$$

where K is a coefficient relating the Reynolds number and the Darcy-Weisbach friction factor. In this study, the coefficient K is derived from a laboratory study of the effects of surface roughness on artificial road surfaces (Katz, 1990), and is expressed as

$$K = 25.17 + \left(\frac{D_{50}}{0.7}\right)^{4.87} + \left(\frac{i}{40}\right)^{3.39} \tag{28}$$

where D_{50} = median soil aggregate diameter, mm
i = rainfall intensity, mm hr^{-1}.

When D_{50} is less than 0.7 mm, it is set equal to 0.7 mm, and when i is less 40 mm hr^{-1} , it is set equal to 40 mm hr^{-1}.

The equilibrium flow depth, h, at the end of a plane can be calculated as

$$h = \left(\frac{rL}{\alpha}\right)^{\frac{1}{m}} \tag{29}$$

where L = plot length, m
α = coefficient
m = exponent.

The exponent and coefficient in equation (29) depend on the roughness equation used. In this case turbulent flow conditions were assumed, and the Darcy-Weisbach equation will be used so that

$$\alpha = \sqrt{\frac{8gS}{f}} \tag{30}$$

and $m = 3/2$.

The three models described above require the determination of the critical shear velocity (u_{*c}) for the large plots. The critical shear velocity is an indicator of the threshold of particle movement marking the transition from interrill to flow-induced erosion conditions. Critical shear velocity can be determined graphically as the point where $q_{sf} = 0$ when plotting q_{sf} versus shear velocity. Shear velocity is calculated as

$$u_* = \sqrt{ghS}. \tag{31}$$

RESULTS AND DISCUSSION

Soil Characteristics

Soil erodibility is related to many soil characteristics. The soil analyses completed in conjunction with this report include only a few of the measurable properties which influence the resistance of soil to both detachment and transport. Table 3 lists summarized soil measurements for the simulator sites.

Soil Gradation Comparisons - Dispersed versus aggregated particle size analysis

Particle size is one of the most fundamental soil factors effecting erodibility. Larger particles are resistant to transport because of the greater force required to entrain them. Very small particles, particulary clay, resist detachment due to their cohesiveness. Therefore the most erodible soils are those which are high in silt and fine sand. Aggregates are also harder to entrain in flow as compared to primary particles due to the aggregate's larger size.

Particle size gradation was determined by both dispersed and aggregated methods. Comparison of the results from each method should provide an indication of the degree of aggregation present in each soil. A lower percentage of coarse material (sand) is expected when using dispersed techniques because the combined effects of chemical dispersant and shaking or mixing the sample prior to sieving aid in breaking down aggregates into smaller particles. All sites did indicate the presence of aggregation with the aggregated

percentage of sand exceeding the dispersed percentage of sand. The Potlatch River and Tee Meadow sites exhibited the most notable difference in aggregated versus dispersed particle size analysis. The aggregated percentage of sand exceeded the dispersed by approximately 54% for both sites. The Tin Cup Creek sites also displayed a high degree of aggregation with about a 30% difference between aggregated and dispersed percent sand. Hahn's Peak and Deep Creek, the coarsest soils included in this study, have a lesser tendency toward aggregation. The difference between aggregated and dispersed sand is approximately 15% for Deep Creek and 7% for Hahn's Peak.

Organic Matter

The organic component of soil is an important factor controlling soil erodibility largely due to its influence on aggregation. The presence of organic products increases the strength and stability of intra-aggregate bonding. All of the soils in this report contained less than 2% organic matter. Hahn's Peak, a coarse sandy loam, had the smallest organic matter content; Tin Cup Creek, a finer loam, had the largest percentage of organic matter.

Volumetric Water Content

Soils which readily absorb and retain water are less erodible than those which absorb water slowly and thereby generate more overland flow. The amount of water retained at a specified pressure, or volumetric water content, is influenced by soil structure

and pore size. Soils with strong aggregation generally have a high volumetric water content. This generalization is borne out by the Potlatch River and Tee Meadow soils which displayed the greatest degree of aggregation and also have the highest volumetric water contents. Hahn's Peak displayed the smallest degree of aggregation and also had the smallest volumetric water content.

Clay Mineralogy

Clay mineralogy influences the stability of soil aggregates. For example, illite and smectite readily form aggregates, but the open lattice structure and shrink/swell characteristics of these minerals make aggregates less stable than those formed with kaolin. The mineralogical analysis of the soils included in this report revealed no measurable amounts of smectite. Kaolin was present in all but one sample in amounts varying from approximately 1.3% at Deep Creek to 3.3% at Tin Cup Creek.

Table 3. Results of soil analyses.

Site	Dispersed Particle Size Analysis			Aggregated Particle Size Analysis		Organic Matter	Volumetric Water Content	Clay Mineralogy	
	Sand %	Silt %	Clay %	Sand %	Silt + Clay %	%	$m^3 m^{-3}$	Kaolin %	Smectite %
Deep Creek 1	71.2	24.8	4.0	85.3	14.7	1.29	0.259	1.3	----*
Deep Creek 2	71.2	24.8	4.0	85.3	14.7	1.29	0.259	1.3	----
Deep Creek 3	71.1	24.1	4.8	86.6	13.4	0.78	0.204	1.2	----
Hahn's Peak 1	83.2	13.4	3.4	90.2	9.8	0.14	0.128	2.3	----
Hahn's Peak 2	83.2	13.4	3.4	90.2	9.8	0.14	0.128	2.3	----
Tin Cup Creek 1	53.5	36.6	9.9	83.3	16.7	1.63	0.231	3.3	----
Tin Cup Creek 2	53.5	36.6	9.9	83.3	16.7	1.63	0.231	3.3	----
Potlatch River 3	22.0	66.9	11.1	76.6	23.4	0.97	0.298	2.8	----
Tee Meadow 5	15.8	76.7	7.5	70.5	29.5	1.39	0.396	----	----

* Dashes (----) indicate that no measurable amount was found.

Rain-induced Interrill Erodibility

Comparison of Equations

The interrill erodibility parameter was computed for the 1 m^2 plots using four different empirical equations. The equations were defined in a previous section. For ease of reference, they are given again in Table 4 and identified with the equation numbers previously assigned. The interrill erosion equations applied in this study were similar in form, but differed slightly in regard to the variables included in each equation. Interrill erodibility is proportional to the inverse of rainfall intensity squared in equations (5) and (8). The difference between the two formulas is the inclusion of a slope adjustment factor, S_f, in equation (8). Equations (10) and (11) are similar in that they both define K_i as being proportional to the inverse of the product of rainfall intensity and rainfall excess. They differ because equation (11) includes S_f.

Table 4. Empirical interrill erosion equations.

Equation	Equation Number
$Ki = \frac{q_{sr}}{i^2 L}$	5
$Ki = \frac{q_{sr}}{i^2 S_f L}$	8
$Ki = \frac{q_{sr}}{irL}$	10
$Ki = \frac{q_{sr}}{irS_f L}$	11

Table 5 lists the computed interrill erodibility parameter values resulting from each interrill erosion equation for the wet and very wet rainfall simulation events. Figure 2 shows a graphical comparison of that data. Each equation produces a unique estimate of interrill erodibility. This result is expected since the computed soil erodibility depends on the form of the interrill erosion equation used. Figure 2 shows that equations (8) and (11) result in parameter estimates approximately twofold that of equations (5) and (10), respectively. This result occurs despite the fact that equations (8) and (11) do not include the same hydrologic variables. Likewise, equations (5) and (10) also do not include the same hydrologic variables.

The similarity of the results of the equation pairs mentioned above can be explained by comparing the measured rainfall intensity and rainfall excess from the forest road plots. In Figure 3, those variables are plotted against each other for both the 1 m^2 and the 5 m^2 plot size. The 1:1 line represents the theoretical line of perfect agreement where rainfall excess would equal rainfall intensity if the road surface was completely impervious. The proximity of all measured data points to the 1:1 line for both plot sizes shows that the rainfall excess rate is not significantly less than the rate of rainfall intensity. This indicates that little infiltration occurred through the compacted road surface. The hydrologic variable in equations (5) and (8) is rainfall intensity squared, while equations (10) and (11) include the product of rainfall intensity and rainfall excess as a hydrologic variable. Because the measured runoff discharge was quite close to rainfall intensity, there is little difference between the value of intensity squared versus the product of intensity

and rainfall excess. Thus the similarity of results from equations (10) and (11) and equations (5) and (8) can be explained.

In this analysis it is not possible to identify one formula as correct and label all others as incorrect. However, some presumptions concerning the conditions affecting erosion on forest roads can be made in selecting one equation to better represent forest road conditions in a process-based erosion model. For example, it has been recognized that erosion in interrill areas results from an interaction between the impacting raindrops and the surface water flow (Kinnell, 1988, 1991). Therefore, the empirical relationships represented in equations (5) and (8) do not enable the effects of surface water flow to be modeled adequately. It can be argued that because forest roads are generally compacted surfaces allowing little infiltration, a large percentage of the rainfall becomes overland flow. According to this reasoning, the rainfall intensity squared term indirectly reflects the generation of surface runoff. However, for the model to be applicable to a broad range of conditions, it is advantageous if it more directly emulates the process it describes.

Slope is generally an important consideration in modeling erosion, but the data in this study represent only a limited range of slopes. Also, the slope adjustment factor (equation (7)) was developed from data gathered from agricultural fields where the effective interrill slopes were very steep, and erosion was probably detachment-limited. Because forest roads are designed to have relatively flat slopes, erosion is more likely to be transport-limited. Because the conditions unique to forest roads are not similar to the conditions under which equation (7) was developed, there are grounds for being suspect

about the use of that equation for forest roads. Therefore, the empirical interrill erosion equations (8) and (11) are judged inappropriate. Equation (5) and (8) were also judged to be inadequate because they do not directly reflect the importance of surface water flow on interrill erosion. Thus equation (10) was selected as the most appropriate choice for further analysis of interrill erosion on forest roads. The rangeland option in the WEPP model also uses equation (10) to represent interrill erosion. In the remainder of this study, equation (10) is used when referring to interrill erosion.

Table 5. Computations for $1m^2$ plot interrill erodibility parameter.

Site	Plot #	Run	Total Sediment Discharge q_{st} kg m^{-1} s^{-1}	Rainfall Intensity i m s^{-1}	Rainfall Excess r m s^{-1}	Slope Factor S_f	EQN 5 Ki_1 kg s m^{-4}	EQN 8 Ki_2 kg s m^{-4}	EQN 10 Ki_3 kg s m^{-4}	EQN 11 Ki_4 kg s m^{-4}
Deep Creek 1	2	W	3.88E-05	9.22E-06	7.74E-06*	0.3943	455938	1156339	543251	1377780
		VW	1.08E-04	8.75E-06	8.02E-06	0.3943	1416947	3593629	1546135	3921274
	3	W	4.75E-05	9.31E-06	7.53E-06	0.3975	548028	1378745	677701	1704982
		VW	4.49E-05	8.36E-06	7.20E-06	0.3975	641890	1614886	745002	1874299
Deep Creek 2	2	W	9.41E-05	1.46E-05	1.25E-05	0.4043	440833	1090456	515148	1274282
		VW	1.09E-04	1.53E-05	1.23E-05	0.4043	463161	1145685	577092	1427508
	3	W	1.24E-04	1.55E-05	1.42E-05	0.3869	516492	1334801	562458	1453594
		VW	1.09E-04	1.52E-05	1.35E-05	0.3869	472758	1221777	533237	1378076
Deep Creek 3	2	W	2.90E-05	9.08E-06	7.59E-06	0.3143	351789	1119099	421188	1339870
		VW	2.51E-05	9.22E-06	7.34E-06	0.3143	294855	937983	370494	1178602
	3	W	2.88E-05	9.08E-06	7.39E-06	0.4268	349371	818598	429619	1006624
		VW	1.09E-05	9.22E-06	7.92E-06	0.4268	128200	300380	149331	349892
Hahn's Peak 1	3	W	1.53E-04	9.78E-06	8.20E-06	0.4502	1596884	3547136	1905047	4231654
		VW	1.32E-04	9.64E-06	8.46E-06	0.4502	1420016	3154261	1618318	3594747
Hahn's Peak 2	3	W	2.48E-04	1.72E-05	1.58E-05	0.3351	835453	2493204	909249	2713429
		VW	2.49E-04	1.71E-05	1.57E-05	0.3351	856746	2556748	929896	2775046
Tin Cup Creek 1	3	W	9.55E-05	9.44E-06	7.00E-06	0.4242	1070975	2524789	1444164	3404569
		VW	1.12E-04	9.17E-06	6.87E-06	0.4242	1333983	3144822	1780659	4197845
Tin Cup Creek 2	3	W	3.34E-04	1.77E-05	1.30E-05	0.5188	1070518	2063341	1451519	2797690
		VW	3.82E-04	1.68E-05	1.39E-05	0.5188	1353510	2608785	1634151	3149701
Potlatch River 3	3	W	9.72E-05	1.80E-05	1.52E-05	0.3518	299145	850220	355186	1009500
		VW	9.71E-05	1.79E-05	1.45E-05	0.3518	303430	862400	373414	1061306
Tee Meadow 5	3	W	7.94E-05	1.29E-05	1.09E-05	0.4141	474129	1145011	562199	1357698
		VW	9.17E-05	1.26E-05	1.17E-05	0.4141	578922	1398083	623222	1505066

Note: W = Wet run, VW = Very Wet run. * Corrected value.

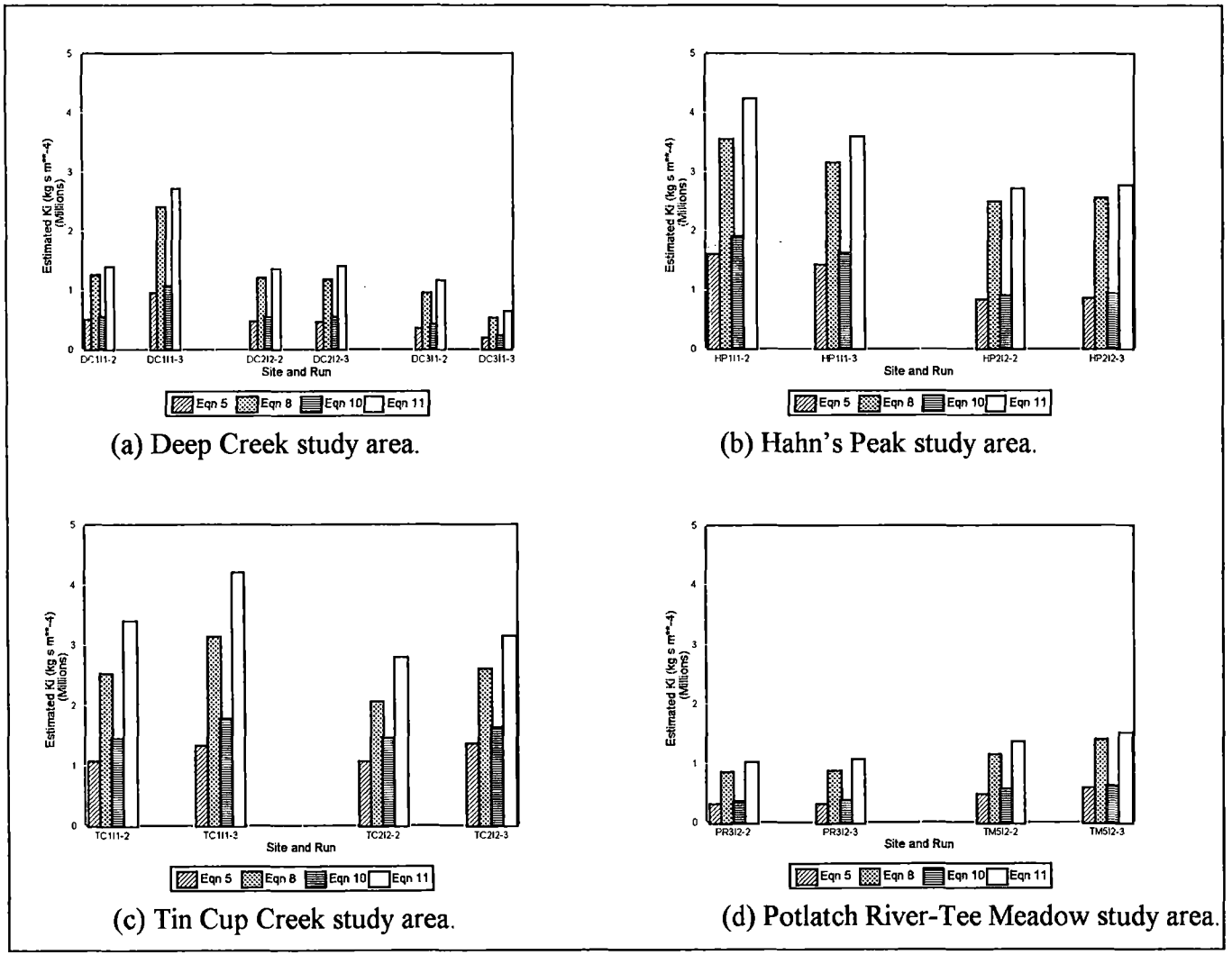

Figure 2. Comparison of four interrill erodibility equations.

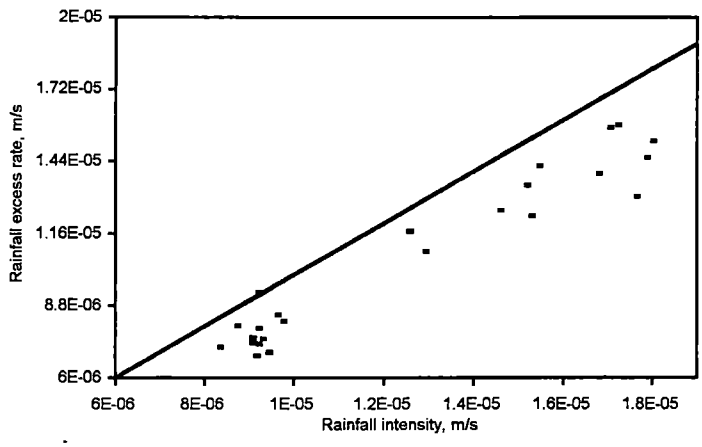

(a) $1m^2$ plots.

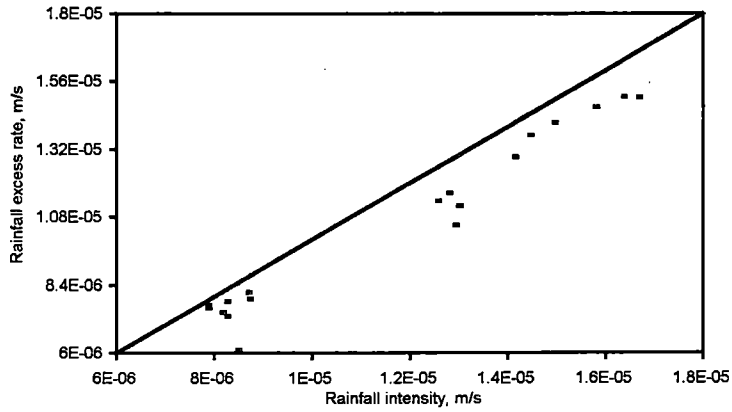

(b) $5m^2$ plots.

Figure 3. Rainfall intensity versus rainfall excess rate.

Predicting Interrill Erodibility

Three regression equations that predict interrill erodibility were applied to the forest road data set. Tables 6 and 7 display the variables required for each equation as well as the resulting predicted soil erodibility parameters. The regression equations presented here were developed for a specific formulation of interrill erodibility as shown in equation (8). As mentioned previously, the interrill erodibility parameter is not only dependent on the soil characteristics, but also depends on the form of the interrill detachment model used. Therefore, the values of interrill erodibility presented in Tables 6 and 7 are specific to the model given in equation (8).

Of the three equations, equation (12) produced the lowest overall values of interrill erodibility. Equation (13) which shares three of the four variables found in equation (12), predicted higher values of the interrill erodibility parameter. Using the results of each equation, the soil for each site can be ranked according to its relative erodibility. Both of these equations rank the Potlatch River-Tee Meadow study areas as the most erodible soil with Tin Cup Creek, Hahn's Peak and Deep Creek having progressively lower soil interrill erodibility.

Both equations (12) and (13) are sensitive to organic matter and volumetric water content variables as demonstrated by the Deep Creek data. Because the first two sites at that study area are in close proximity, they are represented by a single soil sample while a separate soil sample was collected to represent the third site. As can be seen from the soil characterization data in Table 3, the two Deep Creek soil samples are similar in texture but

differ in regard to other variables. The sample representing sites 1 and 2 contained 0.5% more organic matter and had a 5.5% greater volumetric water content than the site 3 soil sample. These differences seem minor when considering that the laboratory tests to determine organic matter and volumetric water content are likely to involve some experimental error. Despite the seemingly minor differences in soil properties, equation (12) predicts a negative value for interrill erodibility for sites 1 and 2, and predicts a positive value for site 3. Equation (13) also behaves erratically by predicting that the site 3 interrill erodibility was nearly 7 times higher than that of sites 1 and 2. The rainfall simulation field data indicate relatively minor differences in soil loss at these three sites. Because the soil characterizations at all 3 Deep Creek sites are basically similar, and because there are no major differences in soil loss between the three sites, it seems likely that the predicted interrill erodibility values should also be similar. The reason for the differences predicted by both equations between sites 1 and 2 versus site 3 lies in the slight differences measured in organic matter and volumetric water content. The sensitivity of these equations to organic matter and volumetric water content is of concern because any experimental error in the laboratory measurement of these soil characteristics is magnified in the estimate of interrill erodibility through the use of equations (12) and (13).

Equations (14a) and (14b) were also applied to the forest road data. The variables pertaining to these equations and the resulting predicted erodibility parameters are shown in Table 7. This equation was tested in two versions. Equation (14a) includes the dispersed silt and clay content as a textural term; equation (14b) contains an undispersed

or aggregated estimate of the silt and clay content. The undispersed silt and clay content was determined using a water stable aggregates procedure. Inclusion of this variable is intended to reflect the effect of aggregation in reducing erodibility. Without dispersion, cohesive soil material maintains an aggregated status and is included in the sand-sized fraction. A large difference between the dispersed and undispersed silt and clay content indicates a high degree of potential aggregation in the soil. The dispersed silt and clay content was approximately 1.5 to 3.5 times higher than the undispersed for all of the soils.

Equations (14a) and (14b) produced different results in terms of relative erodibility ranking. According to equation (14a) which uses a dispersed measure of silt plus clay, Tin Cup Creek is the most erodible soil. Potlatch River-Tee Meadow ranks as the most erodible if aggregated silt plus clay is used (equation (14b)).

The fact that none of the soils in this study contained a measurable amount of smectite clay created a problem with the use of equations (14a) and (14b). That clay mineral is one of the terms in both regression equations; the absence of smectite hinders the use of these equations. In temperate climates conducive to the development of heavy vegetation, illite and kaolinite are the dominant soil minerals. Tropical dry climates are more likely to give rise to smectite clay through the weathering process (Velde, 1992). Thus, smectite clay may not be an important variable to include in an erodibility prediction equation if the overall model is meant to be applied to forests in temperate climates.

As mentioned previously, the predicted erodibility parameter values given in Tables 6 and 7 are specific to the interrill detachment formulation given in equation (8).

Since a different model of interrill detachment (equation (10)) was judged as more appropriate for forest road conditions, the parameter values must be adjusted to reflect this new formulation. These "adjusted" values, as computed by equation (15) are shown in Table 8.

The estimated interrill erodibility parameters given in Table 8 are computed directly from measured field data using equation (10). In Figure 4, the estimated and predicted interrill erodibility values are compared for each of the regression-type erodibility prediction equations. Note that all predicted parameter values shown in Figure 4 have been "adjusted" to be consistent in form with the estimated parameter values. As shown in Figure 4a, equation (12) consistently under predicts the K_i value. Equation (13) also under predicts the erodibility parameter most of the time (Figure 4b). Equations (14a) and (14b) perform slightly better than the other two equations as shown in Figure 4c.

None of the predictive equations examined here provide adequate predictions of forest road soil erodibility as estimated with equation (10). All of the regression equations presented here were developed for other land types. Equations (12) and (13) were developed specifically for rangeland sites in the western United States; equations (14a) and (14b) were developed using data collected from a variety of soils in northern California. However, none of these land types reflect the severely disturbed conditions associated with forest roads. Unique equations developed specifically for forest road sites are necessary in order to adequately predict soil erodibility.

Table 6. Regression equation variables and resulting predicted interrill erodibility parameter from equations (12) and (13).

Site	S_a Sand %	S_i Silt %	O_m Organic Matter %	θ_{fc} Volumetric Water Content %	Equation (12)* Predicted Ki_{p1} kg s^{-1} m^{-4}	Equation (13)** Predicted Ki_{p2} kg s^{-1} m^{-4}
Deep Creek 1,2	71.2	24.8	1.29	25.9	-4.330E+01	3.254E+04
Deep Creek 3	71.1	24.1	0.78	20.4	7.909E+04	2.169E+05
Hahn's Peak 1,2	83.2	13.4	0.14	12.8	3.225E+04	7.849E+04
Tin Cup Creek 1,2	53.5	36.6	1.63	23.1	2.460E+05	6.323E+05
Potlatch River 3	22.0	66.9	0.97	29.8	5.762E+05	1.522E+06
Tee Meadow 5	15.8	76.7	1.39	39.6	5.149E+05	1.438E+06

* Equation (12) $Ki_{p1} = 1000\ (1709 - 1765S_a - 645S_i - 4557O_m - 902\theta_{fc})$

** Equation (13) $Ki_{p2} = 1000\ (3042 - 3166S_a - 8816O_m - 2477\theta_{fc})$

Table 7. Regression equation variables and resulting predicted interrill erodibility parameter from equations (14a) and (14b).

Site	Si + Cl Dispersed Si+Cl %	si + cl Aggregated si + cl %	Ka Kaolin %	Sm Smectite %	Equation (14a)* Predicted Ki_{p3} kg s^{-1} m^{-4}	Equation (14b)** Predicted Ki_{p4} kg s^{-1} m^{-4}
Deep Creek 1,2	28.8	14.7	1.3	0	1.401E+06	8.079E+05
Deep Creek 3	28.9	13.5	1.2	0	1.409E+06	7.505E+05
Hahn's Peak 1,2	16.8	9.9	2.3	0	8.820E+05	5.172E+05
Tin Cup Creek 1,2	46.5	16.7	3.3	0	1.721E+06	8.418E+05
Potlatch River 3	78.0	23.4	2.8	0	1.454E+06	1.153E+06
Tee Meadow 5	84.2	29.5	0	0	1.347E+06	1.469E+06

* Equation (14a) $Ki_{p3} = 1000\ (-25.7 + 69.7(\text{Dispersed Si+Cl}) - 0.6(\text{Dispersed Si+Cl})^2 - 34.3(Ka) + 86.0(Sm))$

** Equation (14b) $Ki_{p4} = 1000\ (-25.7 + 69.7(\text{Aggregated si+cl}) - 0.6(\text{Aggregated si+cl})^2 - 34.3(Ka) + 86.0(Sm))$

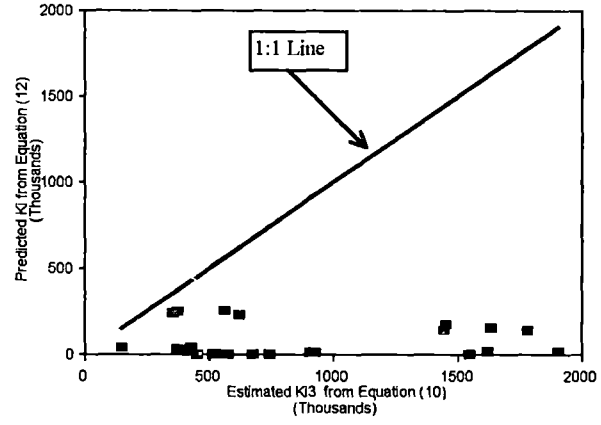

(a) Equation (12)

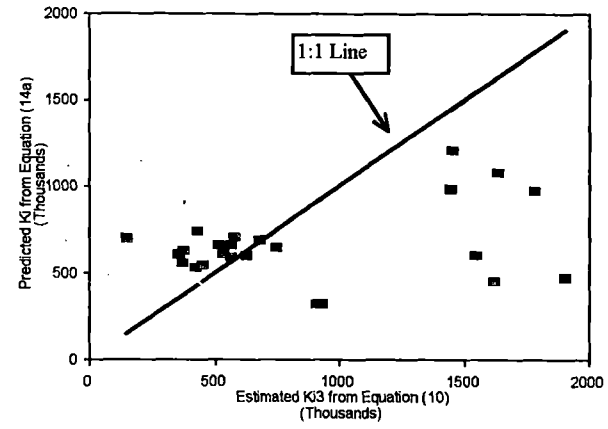

(b) Equation (13)

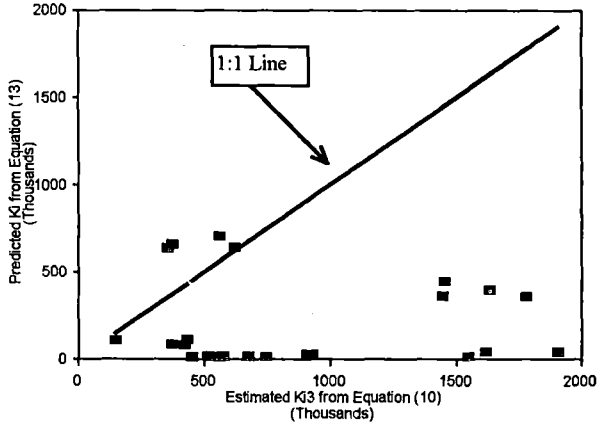

(c) Equation (14a) Dispersed Si+Cl

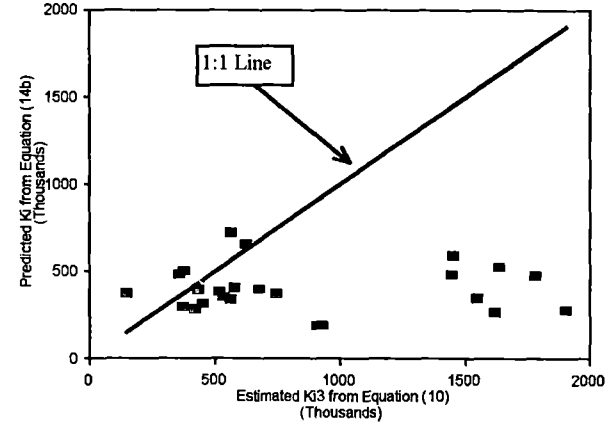

(d) Equation (14b) Aggregated si+cl

Figure 4. Estimated versus predicted interrill erodibility, Ki_3, for the 1 m^2 plots at all study areas.

Table 8. Estimated and predicted interrill erodibility values.

Site	Plot #	Run	Equation (10) Estimated Ki_3 kg s m^{-4}	Equation (12) Predicted Ki_{p1} kg s m^{-4}	Equation (12) Predicted ki_{p1}* kg s m^{-4}	Equation (13) Predicted Ki_{p2} kg s m^{-4}	Equation (13) Predicted ki_{p2}* kg s m^{-4}	Equation (14a) Predicted Ki_{p3} kg s m^{-4}	Equation (14a) Predicted ki_{p3}* kg s m^{-4}	Equation (14b) Predicted Ki_{p4} kg s m^{-4}	Equation (14b) Predicted ki_{p4}* kg s m^{-4}
Deep Creek 1	2	W	543251	1247	486	32539	12675	1401023	545741	807905	314704
		VW	1546135	1247	536	32539	14000	1401023	602781	807905	347596
	3	W	677701	1247	613	32539	15994	1401023	688651	807905	397114
		VW	745002	1247	575	32539	15011	1401023	646339	807905	372714
Deep Creek 2	2	W	515148	1247	589	32539	15372	1401023	661864	807905	381667
		VW	577092	1247	628	32539	16390	1401023	705707	807905	406949
	3	W	562458	1247	525	32539	13711	1401023	590362	807905	340435
		VW	533237	1247	544	32539	14201	1401023	611467	807905	352605
Deep Creek 3	2	W	421188	79867	30059	216901	81634	1408784	530215	750492	282458
		VW	370494	79867	31547	216901	85674	1408784	556455	750492	296437
	3	W	429619	79867	41916	216901	113835	1408784	739363	750492	393876
		VW	149331	79867	39705	216901	107830	1408784	700364	750492	373100
Hahn's Peak 1	3	W	1905047	32394	17398	78490	42154	881958	473670	517246	277796
		VW	1618318	32394	16620	78490	40270	881958	425495	517246	265377
Hahn's Peak 2	3	W	909249	32394	11814	78490	28624	881958	321642	517246	188635
		VW	929896	32394	11782	78490	28547	881958	320770	517246	188124
Tin Cup Creek 1	3	W	1444164	247644	141651	632302	361673	1720927	984360	841765	481184
		VW	1780659	247664	140221	632302	358022	1720927	374422	841765	476623
Tin Cup Creek 2	3	W	1451519	247664	174213	632302	444812	1720927	1210638	841765	592165
		VW	1634151	247664	155125	632302	396076	1720927	1077994	841765	527284
Potlatch River 3	3	W	355186	577166	241116	1521819	635752	1454358	607570	1153378	481833
		VW	373414	577166	249909	1521819	653938	1454358	629728	1153378	499405
Tee Meadow 5	3	W	562199	516271	253488	1438338	706222	1346934	661343	1468545	721054
		VW	623222	516271	230137	1438338	641666	1346934	600421	1468545	654631

W = Wet run, VW = Very Wet Run

*ki_{pn} is the "adjusted" erodibility where $ki_{pn} = Ki_{pn}$ (i/r) S_f.

Flow-induced Erodibility

Determination of Flow-induced Sediment Discharge

As stated previously, the total soil loss from the $5m^2$ plots can be apportioned between that caused by rainfall versus surface flow according to equation (16). The observed interrill erodibility parameter determined from $1m^2$ plot(s) was applied to the $5m^2$ plots to calculate rainfall-induced sediment discharge (q_{sr}). The difference between the total measure sediment discharge (q_{st}) and the calculated q_{sr} can be attributed to the forces of overland flow (q_{sf}).

Table 9 shows that there was flow-induced erosion from the Tin Cup Creek, Hahn's Peak and Potlatch River-Tee Meadow study areas; however, there was no flow-induced erosion on the Deep Creek site. For this reason, the rain-induced sediment discharge is reported as the same value as the total measured sediment discharge for the Deep Creek sites in Table 7.

Parsons and Abrahams (1992) proposed an explanation which may account for the lack of flow-induced sediment discharge at the Deep Creek sites based on the concept that not all of the power of the flow may be available to mobilize particles on the ground surface. The Darcy-Weisbach friction factor (f) can be divided into two constituent factors as

$$f = f' + f'' \tag{32}$$

where f' = grain resistance
f'' = form resistance.

Grain resistance is imparted by erodible soil particles and microaggregates on the soil surface. Form resistance is exerted by microtopographic protuberances like stones and vegetation that are not erodible. In order for soil particles to be entrained, the flow must overcome the total resistance (f). For the forest road plots, form resistance comes from the presence of large gravel and rocks on the road surface. Although the absolute roughness of the forest road sites was not measured, some idea of the roughness associated with each site can be inferred from analysis of the surface composite soil samples. The size of erodible particles will increase as flow intensity increases. For the flow conditions of the forest road plots, rocks greater than 2.5 cm diameter can be considered unerodible. The surface composite samples were collected from the upper 2.5 cm of the road surface, so any large rocks found in the samples were present at the soil surface. The soil samples collected at the Deep Creek sites contained a larger proportion of rocks compared to the other study areas. Over 14% of the sample representing site 3 consisted of rocks greater than 2.5 cm diameter; the sample collected at sites 1 and 2 had nearly 6%. The Tin Cup Creek soil contained some rocks with about 2.5% of the sample greater than 2.5 cm. The Hahn's Peak and Potlatch River-Tee Meadow soil held no rocks of that size. Since the Deep Creek soil contains a considerably larger proportion of unerodible rocks, this soil appears to have a higher form resistance. The dissipation of a large part of the power of overland flow in overcoming form resistance provides an explanation for the apparent lack of flow-induced soil loss at the Deep Creek study area.

Table 9. Sediment discharge for $5m^2$ plots.

Site	Run	Estimated Interrill Erodibility from $1m^2$ plots Ki_3 kg s m^{-4}	Rainfall Intensity i m s^{-1}	Rainfall Excess r m s^{-1}	Sediment Discharge: Rain-induced q_{sr} kg m^{-1} s^{-1}	Sediment Discharge: Flow-induced q_{sf} kg m^{-1} s^{-1}	Sediment Discharge: Total q_{st} kg m^{-1} s^{-1}
Deep Creek 1	W	552500	8.28E-06	7.85E-06	1.89E-04*		1.89E-04
	VW	1073254	7.89E-06	7.61E-06	1.79E-04*		1.79E-04
Deep Creek 2	W	538283	1.58E-05	1.47E-05	6.02E-04*		6.02E-04
	VW	554731	1.50E-05	1.41E-05	5.14E-04*		5.14E-04
Deep Creek 3	W	425383	8.19E-06	7.46E-06	1.17E-04*		1.17E-04
	VW	23521	7.90E-06	7.71E-06	1.23E-04*		1.23E-04
Hahn's Peak 1	W	1905047	8.74E-06	7.94E-06	6.61E-04	1.09E-03	1.75E-03
	VW	1618318	8.71E-06	8.17E-06	5.76E-04	1.38E-03	1.96E-03
Hahn's Peak 2	W	909249	1.67E-05	1.50E-05	1.14E-03	2.63E-04	1.40E-03
	VW	929896	1.64E-05	1.51E-05	1.15E-03	3.44E-04	1.50E-03
Tin Cup Creek 1	W	1444164	8.50E-06	6.13E-06	3.76E-04	8.04E-04	1.18E-03
	VW	1781659	8.28E-06	7.31E-06	5.39E-04	7.59E-04	1.30E-03
Tin Cup Creek 2	W	1451519	1.30E-05	1.12E-05	1.06E-03	1.30E-03	2.36E-03
	VW	1634151	1.28E-05	1.17E-05	1.22E-03	8.12E-04	2.04E-03
Potlatch River 3	W	355186	1.45E-05	1.37E-05	3.53E-04	2.38E-04	5.91E-04
	VW	373414	1.42E-05	1.29E-05	3.42E-04	8.69E-05	4.29E-04
Tee Meadow 5	W	562199	1.29E-05	1.05E-05	3.81E-04	6.00E-04	9.81E-04
	VW	623222	1.26E-05	1.14E-05	4.48E-04	7.23E-04	1.17E-03

Note: W = Wet run, VW = Very Wet run.

* Rain-induced sediment discharge = total sediment discharge as determined by using the interrill erodibility from the 1 m^2 plots and equation (10) to predict the interrill component of 5 m^{2+} plot erosion..

Flow Characteristics

The hydraulic characteristics of flow on the forest road plots are given in Table 10. Flow Reynolds numbers were less than 70, and flow depths were less than 1.0 mm. Since the flows were within the laminar range, discharge per unit width and bedslope can be considered as fundamental hydraulic parameters. Knowing the values of these variables, along with fluid properties and a flow resistance coefficient, it is possible to determine values of most other hydraulic variables, such as boundary shear stress and stream power which are given in Table 11.

Entrainment of soil particles by flow may occur when the actual shear velocity exceeds the critical shear velocity. Figure 5 shows the graphical determination of critical shear velocity. The four points shown on each graph of shear velocity versus flow-induced sediment discharge represent the wet and very wet runs at two sites. The intersection of the best-fit regression line and the x-axis represents the critical shear velocity for that study area.

The shear stress and excess stream power estimated for the flow at the second Hahn's Peak site were less than that for the first although the applied rainfall intensity was greater at the second site. Site 1 received rainfall at a nominal intensity of 30 mm hr^{-1} while a 50 mm hr^{-1} intensity was applied to site 2. The same scenario applies to the Tin Cup Creek study area where site 2 received nearly twice the rainfall intensity as compared to site 1; however, the shear stress and excess stream power estimates are also greater for site 2 as might be expected. The effect of slope may help to explain this anomaly at the

Hahn's Peak study area. The slope of site 1 which received 30 mm hr^{-1} rainfall was nearly twice that of site 2 which received the higher intensity. The difference in slope plays an important role in stream power and shear stress.

Table 10. Flow parameters for $5m^2$ forest road plots.

Site	Run	Kinematic Viscosity ν $m^2 s^{-1}$	Flow Discharge q $m^2 s^{-1}$	Reynold's Number **Re**	Darcy - Weishbach **f**	α ,	Flow Depth **h** m	Average Flow Velocity **u** $m s^{-1}$	Crtitical Shear Velocity u_{*c} $m s^{-1}$
Deep Creek 1	W	1.11E-06	3.93E-05	35	0.7695	2.4069	0.00064	0.0610	0.0189
	VW	1.04E-06	3.81E-05	37	0.7448	2.4464	0.00062	0.0611	0.0186
Deep Creek 2	W	1.11E-06	7.35E-05	66	0.4457	3.2286	0.00080	0.0915	0.0216
	VW	1.04E-06	7.05E-05	68	0.4277	3.2957	0.00077	0.0915	0.0212
Deep Creek 3	W	1.11E-06	3.73E-05	64	0.8097	1.3208	0.00093	0.0402	0.0128
	VW	1.04E-06	3.86E-05	67	0.7352	1.3862	0.00092	0.0420	0.0127
Hahn's Peak 1	W	1.11E-06	3.97E-05	36	0.7608	3.0078	0.00056	0.0711	0.0219
	VW	1.08E-06	4.09E-05	38	0.7211	3.0894	0.00056	0.0731	0.0219
Hahn's Peak 2	W	1.31E-06	7.50E-05	57	0.5250	2.6506	0.00093	0.0808	0.0207
	VW	1.29E-06	7.55E-05	59	0.5106	2.6878	0.00092	0.0817	0.0206
Tin Cup Creek 1	W	1.04E-06	3.07E-05	29	0.9247	2.6844	0.00051	0.0604	0.0206
	VW	1.02E-06	3.66E-05	36	0.7550	2.9706	0.00053	0.0686	0.0211
Tin Cup Creek 2	W	1.02E-06	5.60E-05	55	0.5057	4.5688	0.00053	0.1053	0.0265
	VW	9.35E-07	5.85E-05	63	0.4455	4.8676	0.00053	0.1115	0.0263
Potlatch River 3	W	1.19E-06	6.85E-05	58	0.4968	2.8439	0.00083	0.0821	0.0205
	VW	1.14E-06	6.45E-05	57	0.5022	2.8266	0.00080	0.0802	0.0201
Tee Meadow 5	W	1.02E-06	5.25E-05	51	0.5388	3.0840	0.00066	0.0793	0.0206
	VW	1.03E-06	5.70E-05	55	0.5003	3.2007	0.00068	0.0836	0.0209

Note: W = Wet run, VW = Very Wet run.

Table 11. Shear stress and stream power estimates.

Site	Run	Shear Stress τ $N\ m^{-2}$	Critical Shear Stress τ_c $N\ m^{-2}$	Stream Power Ω	Critical Stream Power Ω_c
Hahn's Peak 1	W	0.4798	0.4098	0.9288	0.7331
	VW	0.4803	0.4097	0.9684	0.7630
Hahn's Peak 2	W	0.4279	0.4101	0.6750	0.6335
	VW	0.4258	0.4101	0.6839	0.6465
Tin Cup Creek 1	W	0.4215	0.0279	0.6396	0.0109
	VW	0.4430	0.0279	0.8055	0.0127
Tin Cup Creek 2	W	0.7000	0.0279	3.0512	0.0243
	VW	0.6903	0.0279	3.2823	0.0266
Potlatch River 3	W	0.4185	0.4006	0.7191	0.6736
	VW	0.4034	0.4006	0.6731	0.6659
Tee Meadow 5	W	0.4230	0.4002	0.8097	0.7450
	VW	0.4360	0.4003	0.8979	0.7898

Note: W = Wet run, VW = Very Wet run.

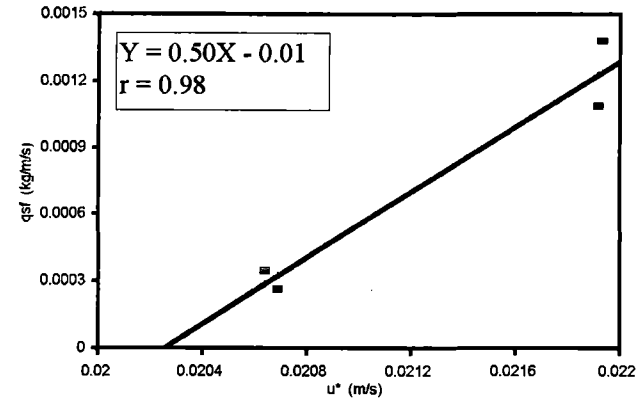

(a) Hahn's Peak, sites 1 and 2.

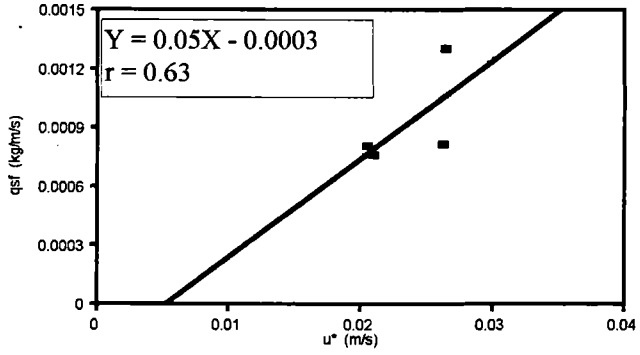

(b) Tin Cup Creek, sites 1 and 2.

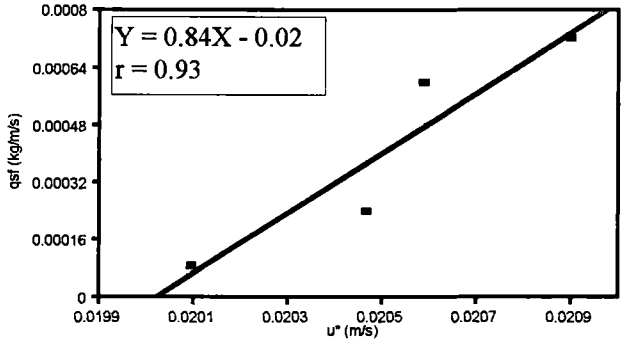

(c) Potlatch River-Tee Meadow, sites 3 and 5.

Figure 5. Graphical determination of critical shear velocity.

Evaluation of Models

Three models of flow-induced soil erodibility were applied to the forest road data set. Each model is a simple exponential equation of the generic form

$$q_{sf} = Kf\,(x)^b \tag{33}$$

where x = model-specific variable
Kf_n = flow-induced soil erodibility
b = exponent.

For ease of reference, Table 12 lists the equations and identifies each with the equation number previously assigned.

Table 12. Flow-induced erodibility equations.

Equation	Equation Number
$Kf_1 = \frac{q_{sf}}{(\Omega_e)^b}$	17
$Kf_2 = \frac{q_{sf}}{(\tau_e)^b}$	21
$Kf_3 = \frac{q_{sf}}{\left(\frac{\tau_e}{D^{.33}}\right)^b}$	22

Effective excess stream power was the model-specific variable (x) for one of the models tested (equation (17)). The other two models relate sediment discharge to effective shear stress. In the first (equation (22)), the effective shear stress is divided by a

measure of mean particle diameter. The final model tested correlates sediment discharge to effective shear stress alone (equation (21)).

Flow-induced soil loss occurred at the Hahn's Peak, Tin Cup Creek and Potlatch River-Tee Meadow study areas. For each of these three study areas, four rainfall simulation events were analyzed to characterize the hydraulics of flow. These four events consist of a wet run and a very wet run, each conducted at two different sites within each study area. Each of the flow-induced erodibility models was fitted to these four points. Graphs of the data and fitted model can be found in Appendix B. The fitted parameter values for these models are given in Table 13. The resulting flow-induced erodibility parameter derived from each model consistently ranks the Hahn's Peak soil as the most erodible, followed by Potlatch River-Tee Meadow and Tin Cup Creek.

The coefficients of determination (r^2) for the fitted models are also given in Table 13. Both of the shear stress models performed equally well. The inclusion of the mean particle diameter term in equation (22) had no significant effect on model performance for this data set. All of the models responded well to the data from Hahn's Peak and Potlatch River-Tee Meadow; however, none of the models yielded a high r^2 for the Tin Cup Creek study area. Less than 30% of the variation in sediment discharge is related to the model variable for the Tin Cup Creek sites. The shear stress and stream power estimates for the Tin Cup Creek sites are considerably higher than the estimates for the other sites in this study. The slope gradient for these plots was also steeper than the slopes of the other plots.

Table 13. Flow-induced erodibility parameters for wet and very wet runs.

Site	b	Kf_1	r^{2*}
Stream Power Model			
Hahn's Peak	0.919052	0.004187	0.97
Tin Cup Creek	0.227022	0.000875	0.20
Potlatch River-Tee Meadow	0.745645	0.003977	0.87
	b	Kf_2	r^{2*}
Shear Stress / D_{50} Model			
Hahn's Peak	1.007804	0.011113	0.95
Tin Cup Creek	0.710163	0.000762	0.28
Potlatch River-Tee Meadow	0.757005	0.003330	0.77
	b	Kf_3	r^{2*}
Shear Stress Model			
Hahn's Peak	1.008074	0.018542	0.95
Tin Cup Creek	0.710229	0.001516	0.28
Potlatch River-Tee Meadow	0.759029	0.009157	0.76

* Note: n = 4 for each study area.

The small amount of data available to evaluate the flow-induced erodibility parameters is of concern. Fitting a model with two parameters to a data set of four points creates uncertainties in the validity of the parameter estimates. The values presented in Table 13 are intended only to provide a basis of comparison for further research.

All of the sediment transport equations presented here are promising models for flow-induced erosion on forest roads. Those equations based on force such as shear stress should be used with care. It may be necessary to make a distinction between the force that is exerted on the bedforms which cannot be eroded and the force that is exerted on the soil particles which can be eroded (Everaert, 1991). Models which include stream

power as a variable are advantageous because bedform roughness is taken into account through the inclusion of mean flow velocity in the stream power calculations.

Summary

The objective of this study was to evaluate the erodibility of the surface of forest roads. Rainfall simulation experiments conducted on forest road surfaces provided the necessary field data. A steady-state process-based approach was used to model the erosion process. Current erosion models, including WEPP, are based on parametric equations that describe the erosion process. Accurate estimation of the parameter values is an essential part of model development. Within that process-based approach, four different empirical equations were chosen to describe rain-induced interrill erosion, and three sediment transport equations were used to describe flow-induced erosion. Each equation was individually evaluated using the forest road data set. Physical and chemical analyses of soil collected at each forest road site was required to characterize the soil properties. Those soil properties were used in existing regression-type equations to predict soil erodibility.

CONCLUSIONS AND RECOMMENDATIONS

From the evaluation of forest road soil erodibility, the following conclusions were obtained:

(1) Because of the small amount of data available, a statistical analysis was not possible. Therefore, no objective means of comparing the various empirical equations existed. However, some reasonable judgments can be made in deciding which equations are most appropriate for use.

(2) Although the data set was small, the estimates of K_i and K_f resulting from this study are useful in establishing a range of values which might be expected from forest roads under similar conditions.

(3) In process-based models, the value of the erodibility parameter depends on the form of the model used. The erodibility parameter values given here cannot be applied directly to other models.

(4)The regression equations which predict interrill erodibility that were tested in this study did not provide accurate estimates of forest road interrill erodibility.

(5) The 5 m^2 plot size was transitional in nature between erosion caused by raindrop impact and erosion due to the forces of flowing water.

In conclusion, this study serves as an important contribution in developing a process-based erosion prediction model for forest roads by providing initial estimates of the erodibility parameters for forest road conditions. To expand on the results of this study, the following topics are suggested fo further investigation:

(1) Conduct additional experiments on forest road interrill areas in order to verify which sediment transport equations presented here are most appropriate.

(2) Use additional data to relate the computed erodibility parameters to site characteristics in order to develop original regression-type equations to predict the erodibility of soils on forest roads.

(3) Incorporate experiments on larger plot sizes to study the integrated effects of both interrill and rill erosion.

REFERENCES

Alberts, E.E., J.M. Laflen, W.J. Rawls, J.R. Simanton and M.A. Nearing. 1989. WEPP Profile Model Documentation. National Soil Erosion Research Laboratory. Report No. 2, U.S.D.A. 6.1-6.15.

Bilby, R.E. 1985. Contributions of road surface sediment to a western Washington stream. *Forest Science*. 31(4):827-838.

Blau, J.B., D.A. Woolhiser and L.J. Lane. 1988. Identification of erosion model parameters. *Transactions ASAE*, 31 (3): 839-854.

Burroughs, E.R., Jr., R.B. Foltz and P.R. Robichaud. 1991. United States Forest Service research on sediment production from forest roads and timber harvest areas. In: *Proceedings of the 10th World Forestry Congress,* Paris, France, pp.187-193.

Burroughs, E.R.,Jr., C.H. Luce and F. Philips. 1992. Estimating interrill erodibility of forest soils. *Transactions ASAE*, 5:1489-1495.

Elliot, W.J., A.M. Liebenow, J.M. Laflen and K.D. Kohl. 1989. A compendium of soil erodibility experiments. Publication No. 3. U.S.D.A. - ARS National Soil Erosion Research Laboratory, West Lafayette, IN.

Everaert, W. 1991. Empirical relations for the sediment transport capacity of interrill flow. *Earth Surface Processes and Landforms*. 16:513-532.

Flanagan, D.C. (editor), 1991. Water Erosion Prediction Project - Hillslope Profile Model Version 91.5 Documentation Corrections and Additions. National Soil Erosion Research Laboratory. Report No. 6, U.S.D.A.

Flanagan, D.C., S.J. Livingston and L.J. Lane. 1993. WEPP Hillslope Profile Erosion Model Version 93.0 User Summary

Foster, G.R. 1982. Modeling the erosion process. In C.T. Haan, H.P. Johnson and D.L. Brakensiek (ed.) Hydrologic Modeling of Small Watersheds, pp.297-380.

Foster, G.R. and L.D. Meyer. 1972. A closed-form soil erosion equation for upland areas. In: H.W. Shen (ed.) *Sedimentation: Symposium to Honor Professor H.A. Einstein,*pp. 12.1 - 12.19. H.W. Shen. Fort Collins, CO.

Foster, G.R., F.P. Eppert and L.D. Meyer. 1979. A programmable rainfall simulator for field plots. In Proceedings of the Rainfall Simulator Workshop, USDA Science and Education Administration, ARM-W-10, pp. 45-59.

Govers, G. 1987. Initiation of motion in overland flow. *Sedimentology*. 34: 1157-1164.

Govers, G. 1992. Evaluation of transporting capacity formulae for overland flow, in Overland Flow Hydraulics and Erosion Mechanics, Edited by A.J. Parsons and A.D. Abrahams, Chapman & Hall, NewYork, NY.

Grossman, R.B., and F.B. Pringle. 1987. Describing soil surface properties - their seasonal changes and implications for management. In Soil Survey Techniques. Soil Science Society of America Special Publication No. 20. pp.57-75.

Guy, B.T., W.T. Dickinson and R.P. Rudra. 1987. The roles of rainfall and runoff in the sediment transport capacity of interrill flow. *Transactions ASAE*, 30 (5):1378-1386.

Guy, B.T., R.P. Rudra and W.T. Dickinson. 1992. Process-oriented research on soil erosion and overland flow, in Overland Flow Hydraulics and Erosion Mechanics, Edited by A.J. Parsons and A.D. Abrahams, Chapman & Hall, NewYork, NY.

Hoover, M.D. 1945. Careless skidding reduces benefits of forest cover for watershed protection. *Journal of Forestry,*. 43(10):765-766.

Katz, D.M. 1990. The effects of surface roughness and rainfall impact on the hydraulics of overland flow. M.S. Thesis, University of Idaho, 110 pp.

Kemper, W.D. and E.J. Koch. 1966. Aggregate stability of soils from the western United States and Canada. USDA-ARS. Tech. Bull. No. 1355. Washington, D.C.: GPO.

Kemper ,W.D. and R.C. Rosenau. 1986. Aggregate stability and size distribution. In Methods of Soil Analysis, Part 1. Physical and Mineralogical Methods, 2nd Ed., 425-442. Madison, WI: Am. Soc. of Agron., Soil Sci. Soc. of America.

Kinnel, P.I.A. 1988. The influence of flow discharge on sediment concentrations in raindrop induced flow transport. *Australian Journal of Soil Research.* 27: 227-233.

Kinnell, P.I.A. 1991. The effect of flow depth on sediment transport iduced by raindrops impacting shallow flows. *Transactions ASAE,* 34 (1): 161-168.

Kinnell, P.I.A. and J.T. Wood. 1992. Isolating erosivity and erodibility components in erosion by rain-impacted flow. *Transactions ASAE,* 35(1): 210-215.

Lane, L.J. and M.A. Nearing, (editors), 1989. WEPP Profile Model Documentation. National Soil Erosion Research Laboratory. Report No. 2, U.S.D.A.

Lane, L.J. and E.D. Shirley. 1982. Modeling erosion in overland flow. In Estimating Erosion and Sediment Yield from Rangelands. USDA Agricultural Reviews and Manuals, ARM-W-26.

Liebenow, A.M., W.J. Elliot, J.M. Laflen and K.D. Kohl. 1990. Interrill erodibility: Collection and analysis of data from cropland soils. *Transactions ASAE*, 33: 1882-1888.

Megahan, W.F., S.B. Monsen and M.D. Wilson. 1991. Probability of sediment yields from surface erosion on granitic roadfills in Idaho. *Journal of Enviromental Quality,* 20:53-60.

Meyer, L.D., G.R. Foster, and M.J.M. Römkens. 1975. Source of soil eroded by water from upland slopes. In: Present and Prospective Technology for Predicting Sediment Yields and Sources, USDA-Agricultural Research Service, ARS-S-40, pp. 177-189.

Meyer,L.D. and W.H. Wischmeier. 1969. Mathematical simulation of the process of soil erosion by water. *Transactions ASAE*, 12(6): 754-758, 762.

Middleton, H.E. 1930. Properties of soils which influence soil erosion. U.S. Dept. Agr., Tech. Bull., 178: 16pp.

Nearing, M.A., L.J. Lane, E.E. Alberts and J.M. Laflen. 1990. Prediction technology for soil erosion by water: Status and needs. *Soil Sci. Soc. Am. J.* 54:1702-1711.

Parsons, A.J. and A.D. Abrahams. 1992. Field investigations of sediment removal in interrill overland flow, in Overland Flow Hydraulics and Erosion Mechanics, Edited by A.J. Parsons and A.D. Abrahams, Chapman & Hall, NewYork, NY.

Rice, R.M., J.S. Rothacher and W.F. Megahan. 1972. Erosional consequences of timber harvesting: An appraisal. In: *National Symposium on Watersheds in Transition* pp. 321-329.

Richards, L.A. 1965. Physical condition of water in soil. In: Methods of Soil Analysis, Part 2. 1st Ed., 128-137. Madison , WI. Am. Soc. of Agron., Soil Sci. Soc. of America.

Trimble, G.R.,Jr. and S. Weitzman. 1953. Soil erosion on logging roads. *Soil Sci. Soc. Proc.* 17(1):152-154

USDA-SCS. 1992. Soil survey laboratory methods and procedures for collecting soil samples. Soil Survey Investigation Report No. 1. USDA, Soil Conserv. Serv., Washington, DC: GPO.

Velde, B. 1992. Introduction to Clay Minerals. Chapman & Hall, London, UK. 198 pp.

Walkley, A. and I.A. Black. 1934. Determination of soil organic matter content. *Soil Science*. 37: 29-38.

Wilkinson, D.F. and J.M. Anderson. 1987. Land and Resource Planning in the National Forests. Island Press, Washington, D.C. 396 pp.

Yoder, R.E. 1936. A direct method of aggregate analysis of soils and a study of the physical nature of erosion losses. *Am. Soc. of Agron. J.* 28: 337-351

APPENDICES

Appendix A. Dispersed Versus Aggregated Particle Size Analysis

Table A1. Dispersed particle size analysis, Deep Creek sites 1 and 2.

Sieve #	Particle Size mm	Mean % Finer by Weight	Standard Deviation* %	Coefficient of Variation %
# 18	1.000	78.54	0.10	0.13
# 40	0.425	62..46	1.08	1.73
# 60	0.250	53.80	0.66	1.22
# 100	0.150	44.87	0.12	0.27
# 200	0.075	34.94	0.30	0.87
Pipet	0.031	26.35	0.15	0.57
Pipet	0.016	18.64	0.33	1.77
Pipet	0.008	13.37	0.21	1.57
Pipet	0.004	10.24	0.30	2.93

* Note: n = 3 replicates.

Table A2. Aggregated particle size analysis, Deep Creek, sites 1 and 2.

Sieve #	Sieve Opening mm	Mean % Finer by Weight	Standard Deviation*	Coefficient of Variation
# 16	1.180	82.45	2.10	2.55
# 30	0.600	65.24	2.25	3.45
# 50	0.300	55.48	3.65	6.58
# 100	0.150	42.91	1.95	4.54
# 200	0.075	23.66	1.24	5.24
# 270	0.053	13.45	0.89	6.62

* Note: n = 8 replicates.

Table A3. Dispersed particle size analysis, Deep Creek site 3.

Sieve #	Particle Size mm	Mean % Finer by Weight	Standard Deviation* %	Coefficient of Variation %
# 18	1.000	82.39	0.69	0.83
# 40	0.425	66.67	0.37	0.55
# 60	0.250	58.21	0.77	1.32
# 100	0.150	49.27	1.41	2.87
# 200	0.075	37.83	3.31	8.75
Pipet	0.031	27.09	0.57	2.10
Pipet	0.016	18.25	1.10	6.03
Pipet	0.008	13.25	0.06	0.45
Pipet	0.004	9.89	0.21	2.12

* Note: n = 3 replicates.

Table A4. Aggregated particle size analysis, Deep Creek, site 3.

Sieve #	Sieve Opening mm	Mean % Finer by Weight	Standard Deviation*	Coefficient of Variation
# 16	1.180	82.45	2.10	2.55
# 30	0.600	65.24	2.25	3.45
# 50	0.300	55.48	3.65	6.58
# 100	0.150	42.91	1.95	4.54
# 200	0.075	23.66	1.24	5.24
# 270	0.053	13.45	0.89	6.62

* Note: n = 8 replicates.

Table A5. Dispersed particle size analysis, Hahn's Peak, sites 1 and 2.

Sieve #	Particle Size mm	Mean % Finer by Weight	Standard Deviation* %	Coefficient of Variation %
# 18	1.000	99.97	0.02	0.02
# 40	0.425	86.49	0.06	0.07
# 60	0.250	56.13	0.96	1.71
# 100	0.150	35.43	0.26	0.74
# 200	0.075	21.45	0.88	4.12
Pipet	0.031	16.91	0.07	0.41
Pipet	0.016	13.79	0.01	0.07
Pipet	0.008	11.36	0.21	1.85
Pipet	0.004	9.23	0.18	1.95

* Note: n = 3 replicates.

Table A6. Aggregated particle size analysis, Hahn's Peak, sites 1 and 2.

Sieve #	Sieve Opening mm	Mean % Finer by Weight	Standard Deviation*	Coefficient of Variation
# 16	1.180	99.70	0.10	0.10
# 30	0.600	96.52	0.59	0.61
# 50	0.300	54.79	1.37	2.50
# 100	0.150	26.35	1.23	4.67
# 200	0.075	13.63	0.29	2.13
# 270	0.053	9.85	0.33	3.35

* Note: n = 8 replicates.

Table A7. Dispersed particle size analysis,Tin Cup Creek, sites 1 and 2.

Sieve #	Particle Size mm	Mean % Finer by Weight	Standard Deviation* %	Coefficient of Variation %
# 18	1.000	97.77	0.06	0.07
# 40	0.425	89.13	0.45	0.51
# 60	0.250	76.58	0.66	0.86
# 100	0.150	64.75	0.08	0.12
# 200	0.075	56.40	0.72	1.28
Pipet	0.031	39.99	0.51	1.28
Pipet	0.016	27.15	0.07	0.26
Pipet	0.008	20.41	0.15	0.73
Pipet	0.004	15.56	0.07	0.45

* Note: n = 3 replicates.

Table A8. Aggregated particle size analysis, Tin Cup Creek, sites 1 and 2.

Sieve #	Sieve Opening mm	Mean % Finer by Weight	Standard Deviation*	Coefficient of Variation
# 16	1.180	93.87	0.52	0.55
# 30	0.600	84.15	1.52	1.81
# 50	0.300	64.76	0.81	1.25
# 100	0.150	41.46	0.75	1.81
# 200	0.075	28.26	0.54	1.91
# 270	0.053	16.70	0.39	2.34

* Note: n = 8 replicates.

Table A9. Dispersed particle size analysis, Potlatch River, site 3.

Sieve #	Particle Size mm	Mean % Finer by Weight	Standard Deviation* %	Coefficient of Variation %
# 18	1.000	97.42	0.04	0.04
# 40	0.425	93.08	0.03	0.03
# 60	0.250	90.43	0.01	0.01
# 100	0.150	88.13	0.01	0.02
# 200	0.075	85.12	0.15	0.17
Pipet	0.031	71.06	0.76	1.07
Pipet	0.016	45.66	0.01	0.02
Pipet	0.008	29.99	0.04	0.13
Pipet	0.004	21.69	0.08	0.37

* Note: n = 3 replicates.

Table A10. Aggregated particle size analysis, Potlatch River, site 3.

Sieve #	Sieve Opening mm	Mean % Finer by Weight	Standard Deviation*	Coefficient of Variation
# 16	1.180	92.54	1.16	1.25
# 30	0.600	71.97	1.94	2.70
# 50	0.300	54.70	2.75	5.03
# 100	0.150	42.95	1.42	3.30
# 200	0.075	32.42	1.50	4.63
# 270	0.053	23.37	0.92	3.94

* Note: n = 8 replicates.

Table A11. Dispersed particle size analysis, Tee Meadow, site 5.

Sieve #	Particle Size mm	Mean % Finer by Weight	Standard Deviation* %	Coefficient of Variation %
# 18	1.000	97.70	0.04	0.04
# 40	0.425	94.27	0.28	0.30
# 60	0.250	92.77	0.41	0.44
# 100	0.150	91.35	0.45	0.50
# 200	0.075	87.53	0.54	0.62
Pipet	0.031	72.53	1.29	1.78
Pipet	0.016	44.01	1.00	2.27
Pipet	0.008	26.03	0.33	1.27
Pipet	0.004	16.87	0.15	0.89

* Note: n = 3 replicates.

Table A12. Aggregated particle size analysis, Tee Meadow, site 5.

Sieve #	Sieve Opening mm	Mean % Finer by Weight	Standard Deviation*	Coefficient of Variation
# 16	1.180	93.22	0.84	0.90
# 30	0.600	82.69	2.22	2.68
# 50	0.300	74.54	1.58	2.12
# 100	0.150	62.03	0.94	1.52
# 200	0.075	53.21	0.67	1.26
# 270	0.053	29.47	1.06	3.60

* Note: n = 8 replicates.

Appendix B. Fitted Sediment Transport Models

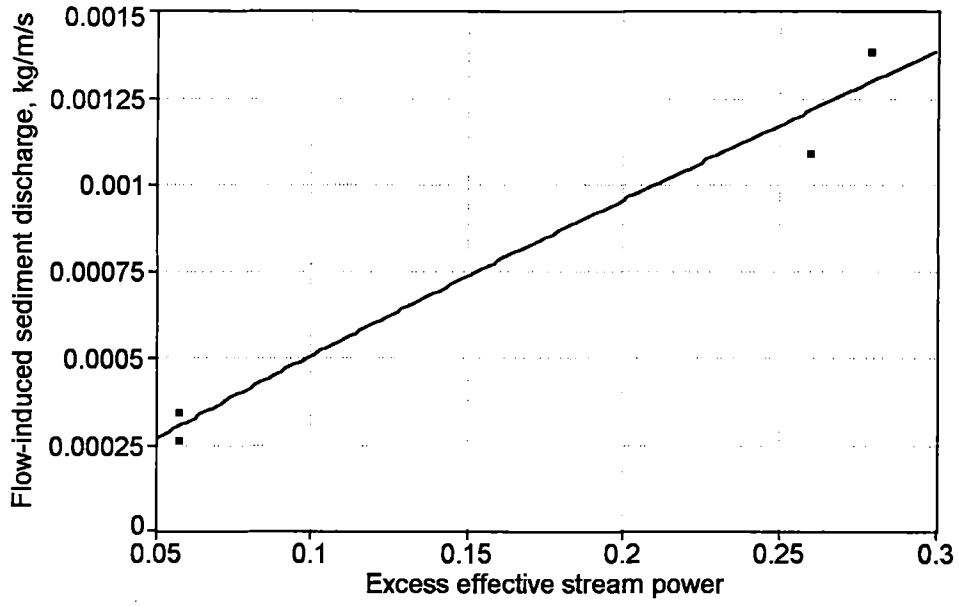

Figure B1. Stream power model, Hahn's Peak study area.

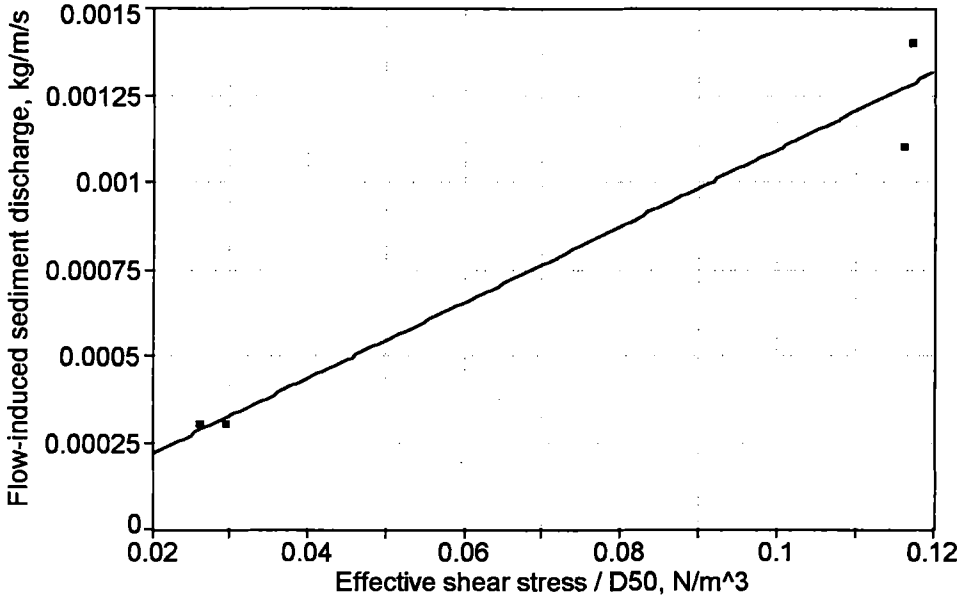

Figure B2. Effective shear stress / D50 model, Hahn's Peak study area.

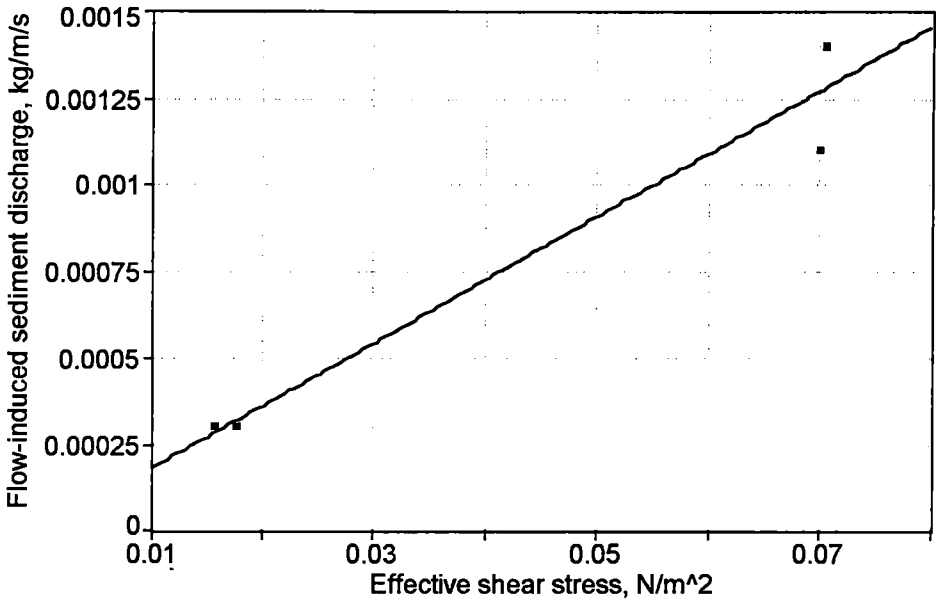

Figure B3. Effective shear stress model, Hahn's Peak.

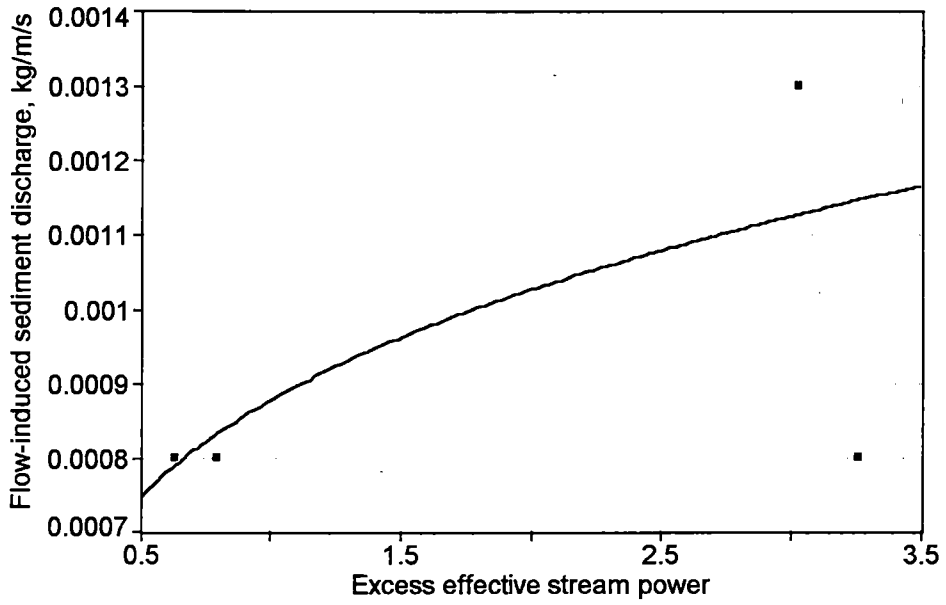

Figure B4. Stream power model, Tin Cup Creek study area.

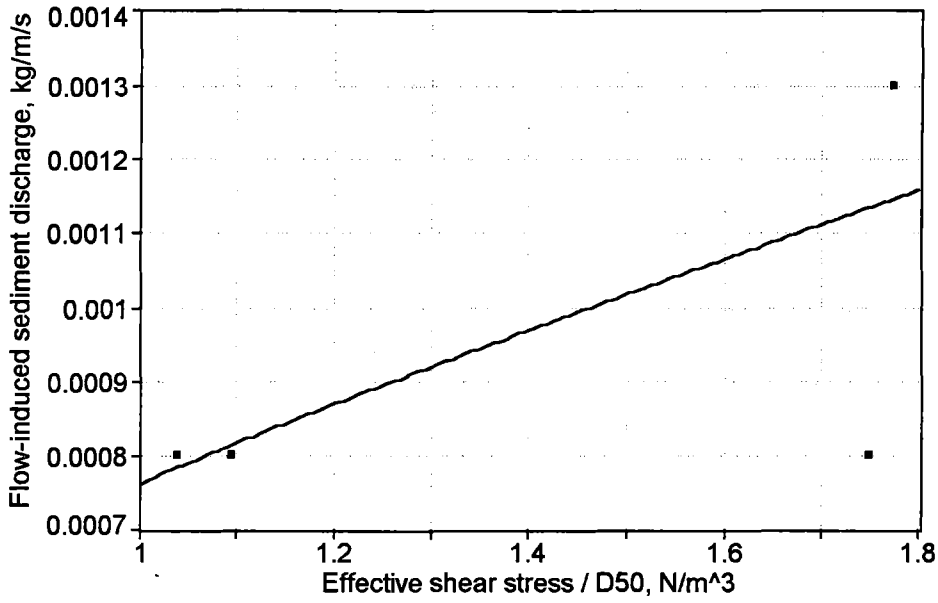

Figure B5. Effective shear stress / D50 model, Tin Cup Creek study area.

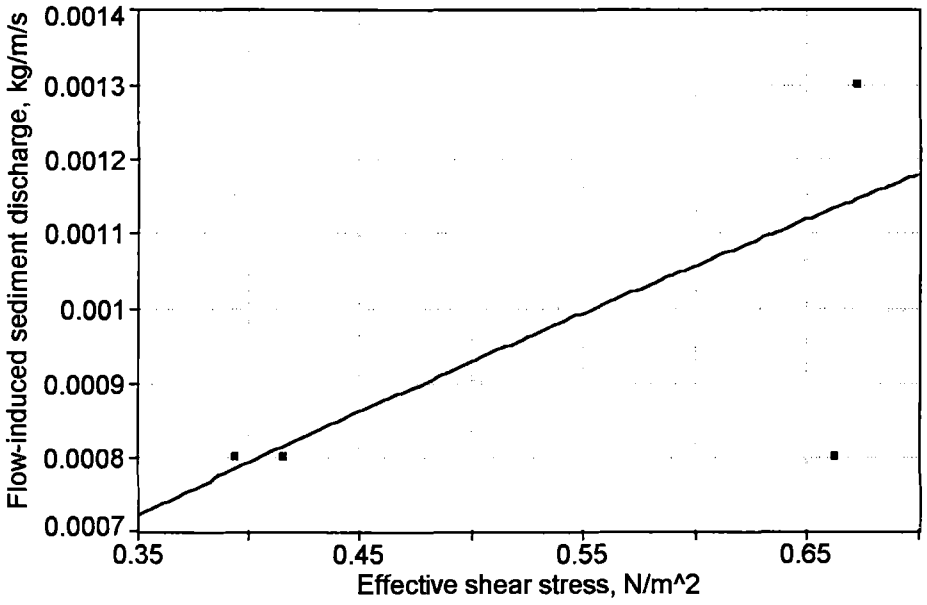

Figure B6. Effective shear stress model, Tin Cup Creek study area.

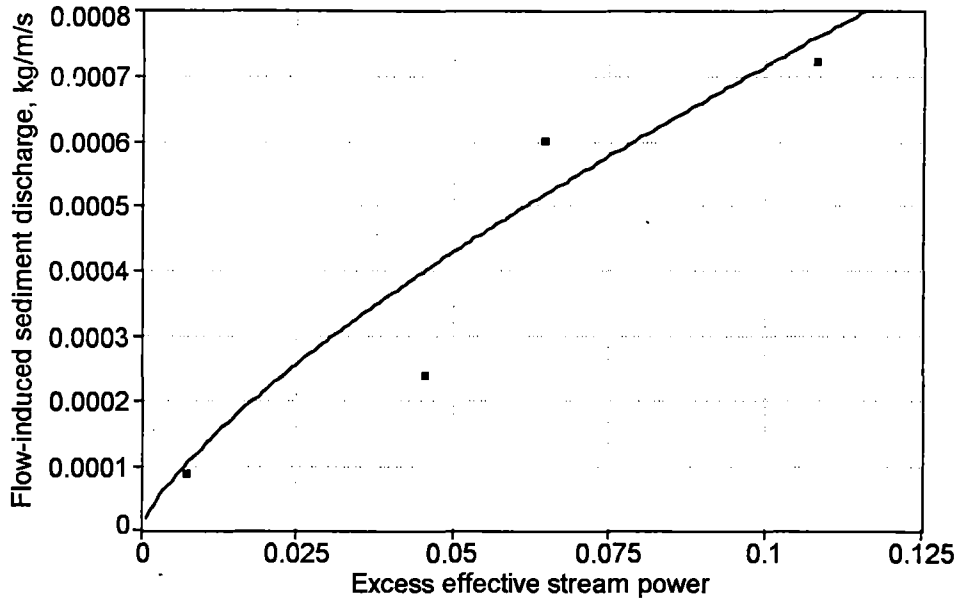

Figure B7. Stream power model, Potlatch River-Tee Meadow study area.

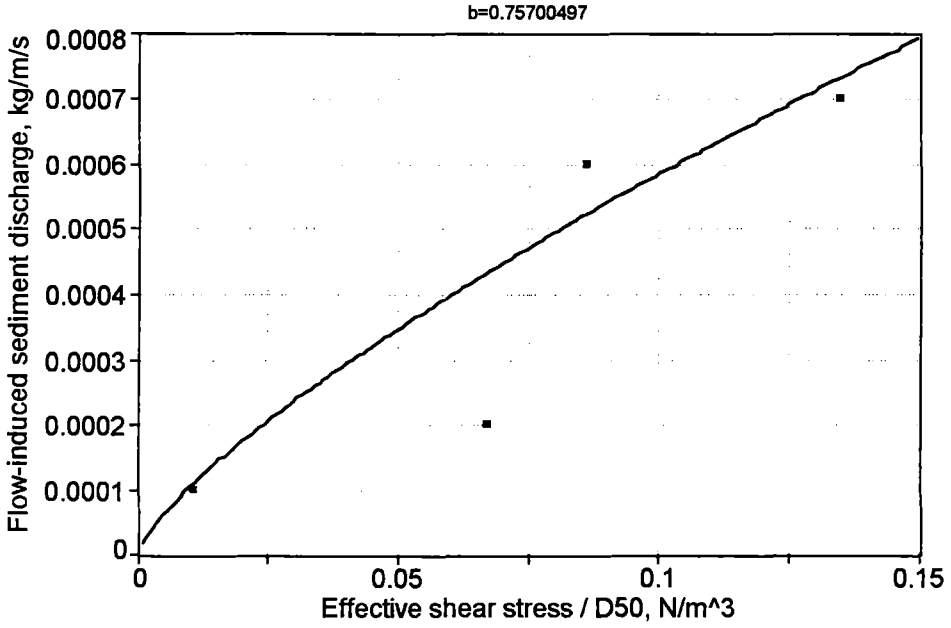

Figure B8. Effective shear stress / D50 model, Potlatch River-Tee Meadow study area.

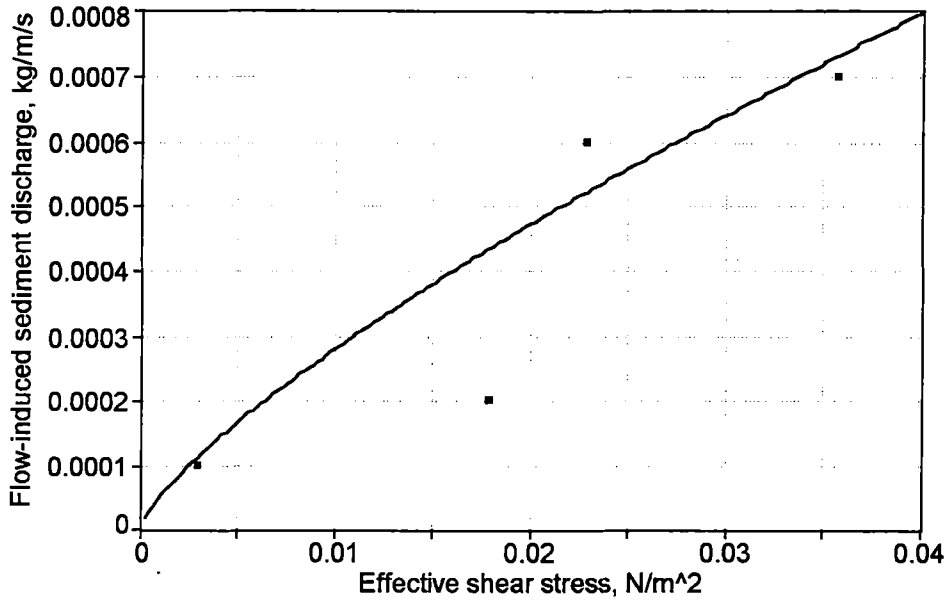

Figure B9. Effective shear stress model, Potlatch River-Tee Meadow study area.

Appendix C: Governing Equations for Sediment Transport Using a Coupled Flow and Raindrop Impact Detachment Model

This report considered the value of erodibility parameters using current and past formulations of the WEPP model. Early in the development of this project, an alternative model was considered, but because the data were insufficient to show that this model was an improvement, further work focussed on finding parameters for the existing WEPP model. This appendix shows the mathematical development of that model in case future work can be done to use it.

The model considers two sources of detachment, flow and raindrop impact. The idea was to have two detachment parameters, one for raindrop impact and one for flow, thus reducing the ambiguity of the WEPP interill erodibility parameter. Transport capacity is modeled only as a function of flow.

The one-dimensional sediment continuity equation given previously was

$$\frac{\partial(ch)}{\partial t} + \frac{\partial(cq)}{\partial x} = D_f + D_i \qquad \text{(C.1)}$$

where h = local flow depth, m

c = sediment concentration, kg m^{-3}

q = flow discharge per unit width, $m^2 s^{-1}$

D_f = detachment or deposition rate due to flow, kg $s^{-1} m^{-2}$

D_i = detachment rate due to raindrop impact, kg $s^{-1} m^{-2}$

x = distance downslope, m

t = time, s

If we consider only steady state, the first term of (C.1) can be dropped, and (C.1) can be rewritten as (Foster and Meyer 1972):

$$\frac{\partial G}{\partial x} = D_f + D_i \tag{C.2}$$

where G = cq = sediment load per unit width, kg s^{-1} m^{-1}

We can further follow the lead of Foster and Meyer (1972) who wrote

$$\frac{\text{Detachment Rate by Flow}}{\text{Detachment Capacity of Flow}} + \frac{\text{Sediment Load of Flow}}{\text{Transport Capacity of Flow}} = 1$$

and write

$$\frac{\text{Detachment Rate by Flow and Raindrop Impact}}{\text{Detachment Capacity of Flow and Raindrop Impact}} + \frac{\text{Sediment Load of Flow}}{\text{Transport Capacity of Flow}} = 1$$

or mathematically

$$\frac{D_f + D_i}{D_{cf} + D_{ci}} + \frac{G}{T_c} = 1 \qquad \text{(C.3)}$$

where D_{ci} = detachment capacity of raindrop impact, kg s^{-1} m^{-2}

D_{cf} = detachment capacity of flow, kg s^{-1} m^{-2}

T_c = Transport capacity of flow per unit width, kg s^{-1} m^{-1}

Equation (C.3) can be solved for $D_i + D_f$ and substituted into (C.2) to give:

$$\frac{\partial G}{\partial x} = \left(D_{ci} + D_{cf}\right)\left(1 - \frac{G}{T_c}\right) \qquad \text{(C.4)}$$

By assigning functions to D_{ci}, D_{cf} and T_c, we can set up a solution to equation (C.4).

The most common type of function for predicting detachment by raindrop impact relates rainfall kinetic energy to detachment with a proportionality as in equations 4 and 6 of the report. Since energy per unit time is power, we suggest a general form with

$$D_{ci} = k_i P \qquad \text{(C.5)}$$

where P is rainfall power per unit area (W m^{-2}) and k_i is a proportionality constant relating rainfall power to detachment rate (s^{-2} m^{-2}). In this type of formulation, any function of rainfall intensity and other precipitation factors can be used to calculate P.

Following the idea of power in detachment, we can use Govers' (1992) relationship for stream power to estimate detachment due to flow energy.

$$D_{cf} = k_f(\Omega - \Omega_{cd}) \tag{C.6}$$

where Ω = effective stream power = $(\gamma SQ)^{3/2}$ $h^{-2/3}$

Ω_{cd} = is the critical stream power required for detachment.

k_f = a proportionality constant between excess effective stream power and detachment by flow.

γ = specific weight of fluid N m-3

S = Ground surface slope

(See pages 25-29 of the report for a more thorough review of Govers' equations)

Because Q and h are both functions of the distance downslope, we can write

$$D_{cf} = D_{cf}(x) \tag{C.7}$$

D_{ci} is a constant in x, so we can write

$$D_{cf} + D_{ci} = D_{cf}(x) + D_{ci} = D_c(x) \tag{C.8}$$

We can likewise use Govers' (1992) stream power relationship to estimate the sediment transport capacity,

$$T_c = k_t(\Omega - \Omega_{ct}) \tag{C.9}$$

where Ω_{ct} = is the critical shear power required for sediment transport.

k_t = a proportionality constant between excess effective stream power and transport capacity

Again, we can write

$$T_c = T_c(x) \tag{C.10}$$

and we can rewrite equation (C.4)

$$\frac{dG}{dx} = (D_c(x))\left(1 - \frac{G}{T_c(x)}\right) \tag{C.11}$$

Rearranging,

$$\frac{dG}{dx} + G\frac{D_c(x)}{T_c(x)} = D_c(x) \tag{C.12}$$

Equation (C.12) is in the form of a linear differential equation which can be solved using an integrating factor, of the form

$$e^{\int \frac{D_c(x)}{T_c(x)} dx}$$

and we find that the steady state sediment load per unit width at the bottom of a uniform slope of length, L, is

$$G(L \quad e^{-\int_0^L \frac{c(}{c(}} \quad e^{\int_0^L \frac{c(}{c(}} \quad \frac{D(x}{T(x} dx \quad c \tag{C.13}$$

which can be solved to any tolerance using numerical integration.